Defence Research and Development Canada
Recherche et développement pour la défense Canada

DEFENCE R&D DÉFENSE

Arctic shoreline delineation & feature detection using RADARSAT-1 interferometry: case study over Alert

Karim E. Mattar and Lloyd Gallop

Defence R&D Canada – Ottawa
TECHNICAL REPORT
DRDC Ottawa TR 2003-225
December 2003

Canada

Arctic shoreline delineation & feature detection using RADARSAT–1 interferometry: case study over Alert

Karim E. Mattar
DRDC Ottawa

Lloyd Gallop
DRDC Ottawa

Defence R&D Canada – Ottawa

Technical Report

DRDC Ottawa TR 2003-225

December 2003

Abstract

Extensive ground truth carried out in and around Alert in 2002 permitting testing the geometric calibration of RADARSAT-1, optimizing the capability of RADARSAT-1 interferometry to delineate coastlines and riverbeds in an Arctic environment, and investigating the detection of various targets and features of potential interest. Surveyed corner reflectors helped demonstrate that a ground reference point greatly improves the geometric calibration of RADARSAT-1 images. A new coherence filter was developed specifically optimized for coastline and riverbed delineation. GPS surveyed coastlines, mapped into radar perspective and calibrated using the surveyed corner reflectors, deviated from the coastline delineated using the coherence filter by less than 8 meters on average. Furthermore, assuming low decorrelation effects, coastlines and riverbeds are often clearly visible in the coherence image, potentially lending the delineation process much more readily to automation. However, RADARSAT-1's fine resolution mode proved too coarse to reliably detect roads, three crashed airplanes and various monuments in the area.

Résumé

Des travaux de vérification importants au sol exécutés en 2002 à Alert et dans les environs nous a permit d'éprouver l'étalonnage géométrique du RADARSAT-1 et d'optimiser l'aptitude du RADARSAT-1 à tracer par interférométrie le trait de côte et les lits de cours d'eau en milieu arctique ainsi que pour étudier la détection de diverses cibles et entités présentant un intérêt potentiel. Des réflecteurs polyédriques dont la position avait été levée ont aidé à démontrer que la présence d'un point de référence au sol améliore considérablement l'étalonnage géométrique des images RADARSAT-1. Un nouveau filtre de cohérence spécifiquement optimisé pour le tracé du trait de côte et des lits de cours d'eau a été mis au point. L'écart entre le trait de côte levé au GPS et cartographié en perspective radar à l'aide des réflecteurs polyédriques de position déterminée et le trait de côte tracé au moyen du filtre de cohérence s'établissait à moins de 8 mètres en moyenne. En outre, en supposant de faibles effets de décorrélation, le trait de côte et les lits des cours d'eau sont souvent nettement visibles sur l'image de cohérence, ce qui pourrait éventuellement permettre d'automatiser beaucoup plus facilement le processus de tracé. Cependant, le mode résolution fine du RADARSAT-1 s'est avéré trop imprécis pour permettre de détecter de manière fiable les sentiers, trois avions écrasés au sol et diverse bornes dans la région

This page intentionally left blank.

Executive summary

This work details a methodology for accurate shoreline delineation in Arctic environments using repeat-pass satellite interferometry. It concludes a study of shoreline delineation using shorelines near Alert, Nunavut as a test site. In the spring and summer of 2002 extensive ground truth was collected in and around Alert, Nunavut and detailed in a technical memorandum [1]. The ground truthing included deployment of four corner reflectors and extensive GPS surveys of coastlines and various targets of potential interest. In conjunction with the ground truth eight interferometric RADARSAT-1 pairs were collected, from which two pairs with the best coherence were selected. This data formed the basis for the study detailed in this report.

This work is a follow-up of two earlier reports that formed part the Global Shoreline project; a project between two agencies, the Defence Research Establishment Ottawa (DREO), Canada and the National Imagery and Mapping Agency (NIMA), USA, initiated in 1998 to study shoreline extraction from imagery. Present day shoreline vector databases have large errors on the order of 500 m. This error is becoming less acceptable as other technologies improve. Other compelling reasons for improving these shoreline estimates include navigational, legal and disaster (e.g. tsunami flood prediction) issues. The first DREO report [3] assessed the utility of polarimetric SAR for shoreline extraction and [4] assessed the utility of RADARSAT-1 interferometric SAR for the same purpose. The purpose of this report is twofold. The main purpose is to develop tools to optimize the accuracy with which shorelines could be mapped using RADARSAT-1 interferometry, with a particular emphasis on shorelines in the Arctic environment. The secondary purpose is to explore target, feature, and road detection with RADARSAT-1 data.

Up to four surveyed corner reflectors were visible in several of the acquired RADARSAT-1 images and permitted evaluation of the geometric calibration accuracy of the images. The 20 measured corner reflectors visible in 7 images were all accurately mapped in the radar slant range perspective to within 4.3 range pixels (approximately 30 meters) and 3.9 azimuth lines (approximately 21 meters). Much greater consistency was observed within passes than between passes, suggesting that the use of one ground control would significantly improve the overall geometric calibration accuracy. Treating one corner reflector per pass as ground control, the geometric calibration accuracy of the remaining corner reflectors improved to within 1.4 pixels in slant range (approximately 10.5 meters) and 0.7 lines in azimuth (approximately 3.7 meters). The consistency of these results should ideally be verified using several different test sites and with surveyed corner reflectors deployed throughout the swath.

To further improve the delineation of coastlines and riverbeds a coherence filter was developed and optimized for this application. The filter was tested using simulated data and demonstrated a ±1 pixel delineation accuracy, a significant improvement compared with standard coherence filters.

Finally the new coherence filter was used to delineate several coastlines near Alert and an accuracy assessment was made. The GPS surveyed coastlines were mapped into the radar perspective, and compare well with the coastlines delineated by the coherence. Over

Williams Island (using GPS data collected under snow covered conditions) the mean deviation between the two coastline measurements was 7.7 m with a standard deviation of 7.8m. Over Sickle Point the mean deviation between the two measurements was 6.7m with a standard deviation of 5.3m.

The study also took advantage of the numerous targets and features of interested that were surveyed and photographed to assess the efficacy of RADARSAT-1 for target and feature detection using the radar amplitude, phase, or coherence, particularly in the Arctic environment. When the decorrelation in the image was low, coherence was found to delineate coastlines and riverbeds much more clearly than the amplitude image, therefore lending itself more readily to automated coastline delineation. However the amplitude, the phase and the coherence had little effect on the detection of the minor roads near Alert. Also, some of the monuments, the 3 crashed airplanes, and the wooden and fibreglass structures in the area were also difficult to detect. With its greater resolution, RADARSAT-2 may be more effective at detecting such targets.

Mattar, K.E., Gallop, L. 2003. Arctic shoreline delineation & feature detection using RADARSAT interferometry: case study over Alert. DRDC Ottawa TR 2003-225. Defence R&D Canada – Ottawa

Sommaire

Ces travaux détaille un méthodologie pour optimiser l'exactitude avec laquelle le trait de côte peut être cartographie par l'interferometry par satellite à passage rèpètè. Ils termines un étude de définir le littoral a l'environnant d'Alert, Nunavut. Au printemps et à l'été de 2002, d'abondantes données de vérification au sol ont été recueillies à Alert et dans les environs, au Nunavut, et présentées dans un document technique détaillé. Les travaux de vérification au sol ont englobé l'installation de quatre réflecteurs polyédriques et des levés GPS de longs segments du trait de côte ainsi que de diverses cibles d'intérêt potentiel. En conjonction avec cette vérification au sol, on a acquis huit couples interférométriques RADARSAT-1. Ces données sont à l'origine de l'étude documentée dans le présent rapport.

Ces travaux font suite à deux rapports antérieurs rédigés dans le cadre du Global Shoreline Project, lancé conjointement en 1998 par le Centre de recherches pour la défense Ottawa (CRDO) du Canada et la National Imagery and Mapping Agency (NIMA) des É.-U. afin d'étudier l'extraction du trait de côte de l'imagerie. De nos jours, les bases de données de vecteurs de la ligne de rivage présentent des erreurs importantes de l'ordre de 500 m. L'amélioration des autres technologies rend cette erreur de moins en moins acceptable. Il y a d'autres raisons pour nous convaincre d'améliorer ces estimations de la ligne de rivage, notamment la navigation, l'aspect juridique et les catastrophes (ex. : la prédiction des inondations des tsunamis). Dans le rapport CRDO précédent on évaluait l'utilité des images RSO polarimétriques et des images RSO interférométriques du RADARSAT-1 pour l'extraction du trait de côte. L'objectif principal est la mise au point d'outils visant à optimiser l'exactitude avec laquelle le trait de côte peut être cartographié par interférométrie RADARSAT-1 en plaçant l'emphase sur les littoraux en milieu arctique. Un objectif secondaire consiste à explorer la détection de cibles, d'entités et de sentiers au moyen des données RADARSAT-1.

Jusqu'à quatre réflecteurs polyédriques dont la position avait été levée étaient visibles sur plusieurs des images RADARSAT-1 acquises et permettaient l'évaluation de l'étalonnage géométrique des images. Les 20 réflecteurs polyédriques dont la position avait été déterminée qui étaient visibles sur 7 images ont tous été cartographiés avec exactitude suivant la perspective en distance-temps à moins de 4,3 pixels près en distance (approximativement 30 mètres) et à moins de 3,9 lignes près en azimut (approximativement 21 mètres). Une beaucoup plus grande uniformité a été observée à l'intérieur d'un même passage que d'un passage à l'autre, ce qui suggère que l'utilisation d'un point d'appui au sol améliorerait considérablement l'exactitude globale de l'étalonnage géométrique. Le traitement d'un réflecteur polyédrique par passage comme référence-terrain améliorait l'exactitude de l'étalonnage géométrique des autres réflecteurs polyédriques pour le porter à moins de 1,4 pixel près en distance-temps (approximativement 10,5 mètres) et à moins de 0,7 ligne près en azimut (approximativement 3,7 mètres). L'uniformité de ces résultats devrait idéalement être vérifiée à plusieurs emplacements d'essai et avec des réflecteurs polyédriques installés sur toute la largeur de la fauchée.

Afin d'améliorer davantage le tracé du trait de côte et des lits des cours d'eau un filtre de cohérence a été conçu et optimisé pour cette application. Le filtre a été mis à l'épreuve avec

des données simulées et a permis d'obtenir un tracé exact à un pixel près, ce qui représente une amélioration importante par rapport aux filtres de cohérence ordinaires.

Enfin, le nouveau filtre de cohérence a été utilisé pour tracer plusieurs segments du trait de côte près d'Alert et on a effectué une évaluation de l'exactitude obtenue. Le trait de côte levé au GPS a été cartographié dans la perspective radar et se compare favorablement au trait de côte tracé par cohérence. Sur l'île Williams (d'après des données GPS recueillies en présence d'une couverture nivale), l'écart moyen entre les deux mesures du trait de côte obtenu était de 7,7 m avec un écart-type de 7,8 m. Sur la pointe Sickle, l'écart moyen entre les deux mesures était de 6,7 m avec un écart-type de 5,3 m.

Dans le cadre de cette étude on a en outre tiré avantage de nombreuses cibles et entités d'intérêt qui ont été levées et photographiées dans le but d'évaluer l'efficacité du RADARSAT-1 pour la détection de cibles et d'entités, en particulier en milieu arctique. Lorsque la décorrélation pour l'image était faible, on a constaté que la cohérence permettait de tracer le trait de côte et les lits des cours d'eau beaucoup plus nettement que l'image de l'amplitude, ce qui pourrait éventuellement permettre d'automatiser plus facilement le processus de tracé. On a cependant noté que l'amplitude, la phase et la cohérence étaient inefficaces pour le tracé des sentiers et des chemins secondaires près d'Alert. Certaines des bornes, les trois avions écrasés et les structures en bois et en fibre de verre dans la région d'étude étaient également difficiles à détecter. Avec sa résolution supérieur, RADARASAT-2 peux être meilleur.

Mattar, K.E., Gallop, L. 2003. Arctic shoreline delineation & feature detection using RADARSAT interferometry: case study over Alert. DRDC Ottawa TR 2003-225. R & D pour la défense Canada - Ottawa

Table of contents

List of figures

List of tables

Acknowledgements

We would like to acknowledge J. Lang for collecting the ground truth and pictures in Alert in the spring and summer of 2002, and the great assistance of Maureen Yeremy in planning the mission. We are grateful to the CFS Alert personnel for their general support throughout these missions. The RADARSAT-1 SAR data are copyright CSA (Canadian Space Agency), 2002.

Introduction

Due to its climate and geology, the Arctic poses unique challenges to mapping and monitoring. Accurate and consistent delineation of its coastlines and lakes has proven particularly difficult, especially considering the profusion of lakes and variety of shorelines that make up the Canadian Arctic. The current accuracies of the global vector shoreline database are on the order of ±500 meters. An earlier report [4] explored the use of coherence for shoreline delineation and lake extraction. It determined that coherence potentially provided a valuable shoreline delineation tool that could be used to improve the shoreline vector database in Arctic environments. The purpose of this report is twofold. (1) Its main purpose is to assess, and develop tools to optimize, the accuracy with which arctic shorelines could be delineated and mapped using satellite (in this case RADARSAT-1) interferometry under different seasonal conditions. (2) The large extent of the ground truth collected permitted expansion of the original study to include an assessment of targets, features, and trail detection under both winter and summer conditions using RADARSAT-1 data.

A unique opportunity arose in 2002 to collect ground truth in and around Alert, Nunavut (see Figure 1). A group of researchers from Ottawa and our facility had plans to conduct experiments in Alert in the spring and again in the summer. By piggybacking on this other activity, expenses were minimal and extensive ground truth was collected. The ground truth included ground and aerial photographs, a GPS survey of coastlines, lakes, roads, and monuments, and deployment and survey of up to four radar corner reflectors. These are described in detail in a technical memorandum [1].

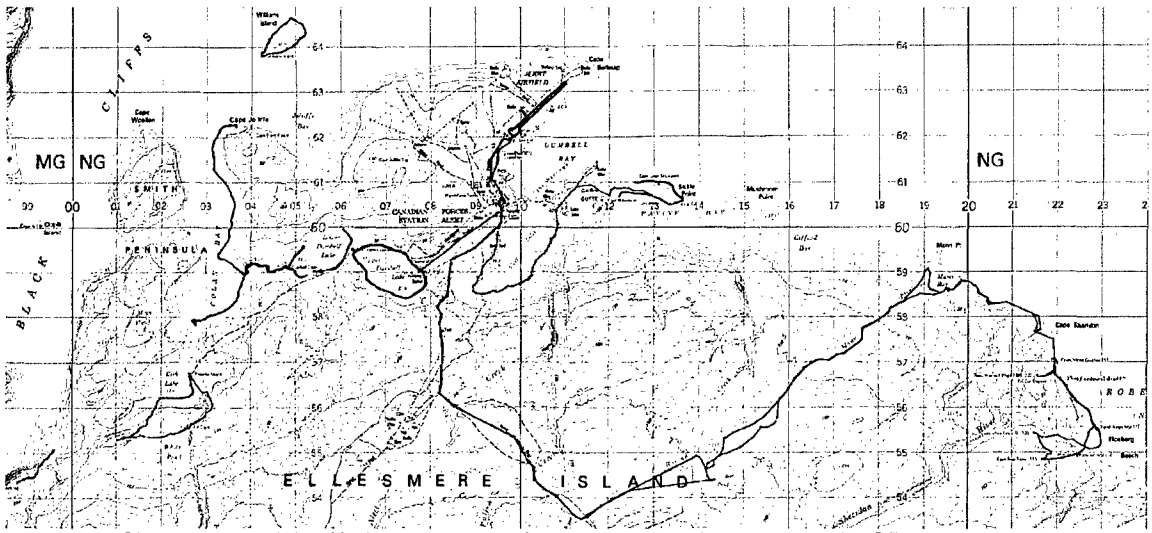

Figure 1: Site overview of the Alert ground truth missions. The roads traversed with GPS are marked in blue.

This report is divided into 8 sections. After this brief introduction, we discuss the collection and processing of the RADARSAT-1 interferometry data collected over Alert. We explore the horizontal mapping accuracy, we propose a new coherence filtering designed to accurately delineate linear changes in the coherence, and we discuss target and feature detection, as well

as shoreline and trail detection. We end the report by detailing the achieved shoreline delineation accuracy and conclude with a summary.

Potential utility to the military

Interferometric coherence, derived from RADARSAT-1, RADARSAT-2, or ERS-1/2 tandem interferometry, is potentially a valuable tool for greatly improving the accuracy of the vector shoreline database in the Canadian Arctic in particular, and Arctic environments in general. Data processing for shoreline extraction can potentially be streamlined and largely automated. Since terrain elevation at the shoreline is obviously known, traditionally the most time consuming and manually intensive portions of interferometric SAR processing chain, namely phase unwrapping and absolute phase calibration, are not required for this application. The 50 km swath width of RADARSAT and 100 km swath width for ERS permits coverage of large portions of terrain in a single mission. Furthermore, interferometric data are already available for large portions of the Canadian Arctic. RADARSAT-1 collected interferometric pairs using the fine resolution mode over large portions of the Canadian Arctic in the fall of 2000 during the Canadian Space Agency's (CSA) Canadian Interferometric Mission (CIM). During its lifetime from March 1995 to March 2000 ERS-1/2 tandem mission also collected large volumes of interferometric data over the region.

Interferometric coherence has other potentially valuable applications to the military. These include lake masking, road and riverbed mapping, and change detection. Several of these applications, target detection with coherence in particular, will benefit from the higher, 3-meter resolution (and multi-polarimetric capability) of RADARSAT-2.

The arid nature of the Arctic makes it a very favourable environment for this technology. At C-band, the wavelength at which RADARSAT-1/2 and ERS-1/2 operate, movement of trees in a forest cause loss of coherence in repeat-pass interferometry. Changes in terrain moisture between the two passes, due to rain or flooding, will also cause loss of coherence. Both of these sources of incoherence are minimized the Arctic environment. On the other hand, a few applications have benefited from such loss of coherence. Coherence has been used to map natural disasters such as floods. Monitoring the coherence of a particular terrain can help analysis of the terrain type and moisture content of the soil for ascertaining cross-country vehicle mobility.

Alert RADARSAT-1 interferometry data

Numerous problems were encountered in acquiring the RADARSAT-1 images. Several planned image acquisitions were lost due to "satellite anomaly". Other problems arose because Alert in not visible from the Canadian ground stations and therefore we had to rely on the tape recorders on board the satellite recording the data. Because of the age of the tape recorder aboard the satellite, CSA recently adopted the policy of downloading the tape recorder only sparingly. This resulted in a few more of our acquisitions being lost because of a full tape recorder. Since we are only interested in interferometric pairs, the loss of one acquisition resulted in the loss of the interferometric pair.

A complete list of images finally acquired is provided in Table 1. All effort was made to acquire the images while the ground truth was being collected and the corner reflectors deployed. Between 2 and 4 corner reflectors are visible in three of the images acquired in the spring and three acquired in the summer (see the last column of Table 1).

Table 1: RADARSAT-1 data acquisition over Alert

INTERFEROMETRIC PAIR (2002)	DAY OF THE YEAR (2002)	START TIME (GMT)	BEAM POSITION	INCIDENCE ANGLE AT SCENE CENTRE (DEGREES)	PASS	ORBIT #	NUMBER OF VISIBLE CORNER REFLECTORS
Mar 23	082	12:00:50.669	F1F	39.232	Desc	33313	0
Apr 16	106	12:00:49.789	F1F	39.232	Desc	33656	0
Apr 13	103	11:48:21.211	F2F	41.475	Desc	33613	4
May 7	127	11:48:15.295	F2F	41.475	Desc	33956	4
Apr 20	110	11:44:07.243	F2F	41.479	Desc	33713	0
May 14	134	11:44:04.704	F2F	41.479	Desc	34056	4
Jul 27	208	20:45:46.909	F3F	43.412	Asc	35119	0
Aug 20	232	20:45:42.970	F3F	43.412	Asc	35462	0
Jul 30	211	20:58:19.350	F4F	45.275	Asc	35162	2
Aug 23	235	20:58:23.750	F4F	45.275	Asc	35505	0
Aug 4	216	11:52:20.004	F2N	40.060	Desc	35228	4
Aug 28	241	11:52:18.368	F2N	40.060	Desc	35571	0
Aug 5	217	11:23:01.703	F4N	44.126	Desc	35242	2
Aug 29	242	11:22:59.958	F4N	44.126	Desc	35585	0
Aug 8	220	11:35:34.371	F3	42.809	Desc	35285	0
Sep 1	244	11:35:33.357	F3	42.809	Desc	35628	0
Oct 30	303	11:15:30.38	F5	46.500	Desc	36471	0
Jan 10 '03	10	11:14:24.594	F5	46.500	Desc	37500	0
Feb 3	34	11:14:20.524	F5	46.500	Desc	37843	0
Feb 27	58	11:14:17.446	F5	46.500	Desc	38186	0
Mar 23	82	11:14:17.110	F5	46.500	Desc	38529	0

The orbit of RADARSAT-1 necessitates that interferometric pairs be collected 24 days apart (or larger integer multiples of 24). In total, three interferometric pairs were acquired in the spring and five in the summer.

The seven remaining interferometric pairs were focused and processed to single look complex (SLC) using MacDonald Dettwiler's (MDA's) "PGS" software. Data formatting problems with one of the summer images resulted in the loss of one of the five pairs. We relied on in-house software for the remainder of the interferometric processing. This included azimuth spectral filtering to improve the coherence, fine registration of the designated slave to its master (to 1/8 of a pixel or line), removal of the flat-earth component of the phase from the designated slave, and finally formation of the interferogram and calculation of the coherence. The processing also included an estimation of the perpendicular baseline ($B_\perp$, the distance between the master and slave satellites in the direction perpendicular to the master to target range), calculation of the target height that would cause a 2π change in the interferometric phase, and an estimation of the ionospheric effects (see [2]). The results of the interferometric processing are summarised in Table 2. In all cases, ionospheric effects were present but were too weak to cause a noticeable degradation of the coherence.

Table 2: RADARSAT-1 interferometric pairs, Alert 2002

INTERFEROMETRIC PAIR (2002)	$B_\perp$ (M)	2π HEIGHT AMBIGUITY AT SCENE CENTRE (M)	GENERAL COHERENCE OVER ALERT	GROUND RANGE SPACING: NEAR TO FAR RANGE (M)	AZIMUTH SPACING (M)
Mar 23–Apr 16	128	144	Poor	7.2-7.5	5.14
Apr 13–May 7	47	402	Good	7.2-6.9	5.28
Apr 20–May 14	155	121	Good	7.2-6.9	5.28
Jul 27–Aug 20	151	136	Poor	6.6-6.9	4.84
Jul 30–Aug 23	–	–	–	6.4-6.6	4.96
Aug 4–Aug 28	114	190	Good	7.1-7.4	5.29
Aug 5–Aug 29	147	141	V Good	6.6-6.8	4.96
Aug 8–Sep 1	209	95	V Good	6.7-6.9	4.85

Of the three interferometric pair acquired in the spring (i.e. under winter, snow-covered conditions), the April 20 – May 14 was the best. It had the best balance of good coherence in the region of interest, large perpendicular baseline to accentuate elevation changes, and good coverage of all the areas of interest.

The amplitude, phase (with amplitude as the background) and coherence for this pair are shown in Figure 2. The amplitude is from April 13, the designated master of the pair. As expected, it clearly shows the sea ice and the patterns in the sea ice, which at this time of the year covers the entire sea visible in the scene. The phase is proportional to the ground topography. One cycle of colour is equal to a phase change of 2π and equivalent, at scene centre, to an elevation change of 121 meters.

The coherence is generally high on the land and low in the sea. It is therefore a good tool for detecting shorelines. The small island left of scene centre shows up clearly in the coherence image. It is barely visible in the phase image and is indistinguishable from the sea ice in the amplitude image. The coherence image also distinguishes 2 regions of sea ice. The more stable portion of the sea ice has a relatively higher coherence than the relatively unstable portion (given the 24 days that separate the pair). The coherence image is also the best of the three for accentuating the river and drainage network. Snow precipitation or drifting snow often causes a degradation of the coherence in Arctic environments. Weather reports from Alert (see [1]) show little precipitation but strong gusts of wind. Strong winds often cause snow drifts and snow accumulation in the drainage networks. This may explain the larger loss of coherence in the drainage networks compared with open terrain.

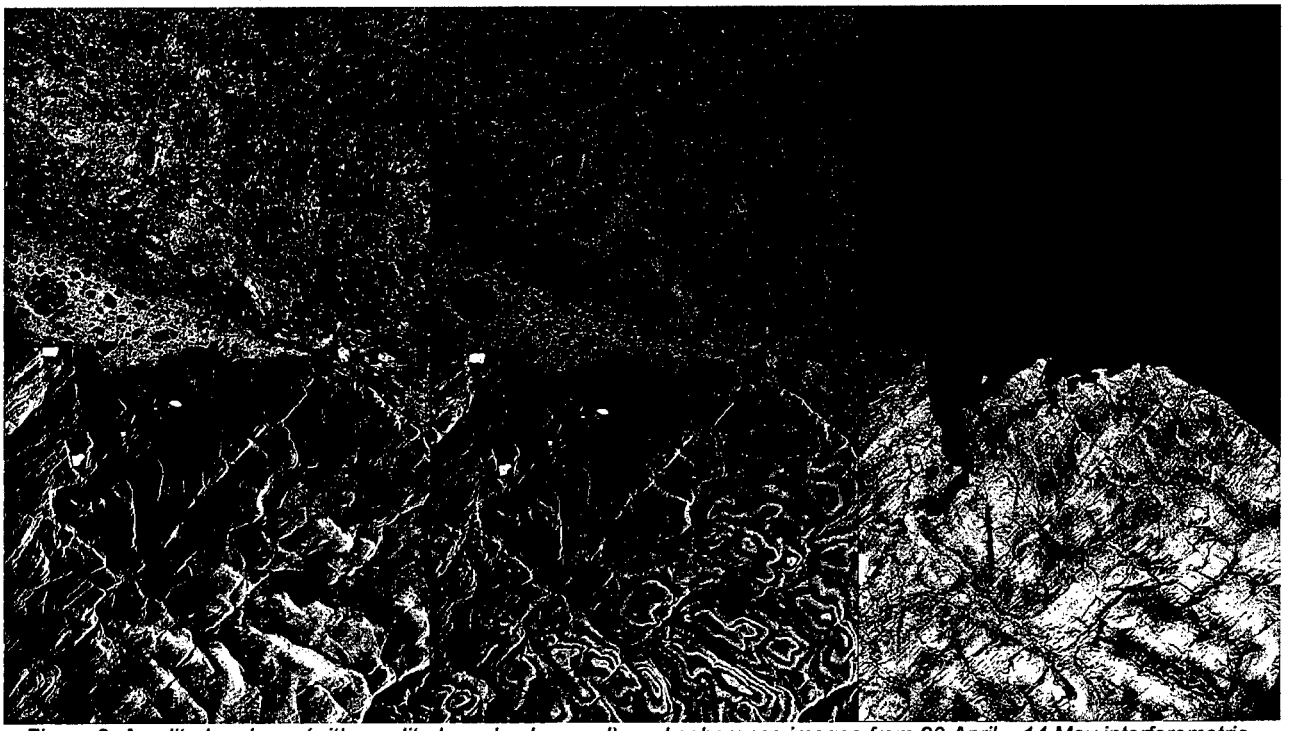

Figure 2: Amplitude, phase (with amplitude as background), and coherence images from 20 April – 14 May interferometric data. The image covers an area of approximately 79 km x 42 km. Near range is on the right.

Of the interferometric pairs acquired in the summer, the August 8 – September 1 pair was by far the best. It has the largest perpendicular baseline, generally very good coherence, and good coverage. Unfortunately it was not acquired while the corner reflectors were deployed. The August 4 image, with four corner reflectors visible over a wide area, is the best for applications where clearly visible reference targets are required. Notice that, even in the summer, sea ice is visible in the amplitude image and along some of the shorelines. The same island referred to previously is barely visible in the amplitude image, yet again is clearly visible in the coherence image. The riverbeds and drainage networks are again well outlined in the coherence image, or at least in the upper portion of the image. The lower portion of the image suffers from a loss of coherence, probably due to precipitation in that area at or close to one of the acquisition dates. The Alert weather station reported an unusually dry summer.

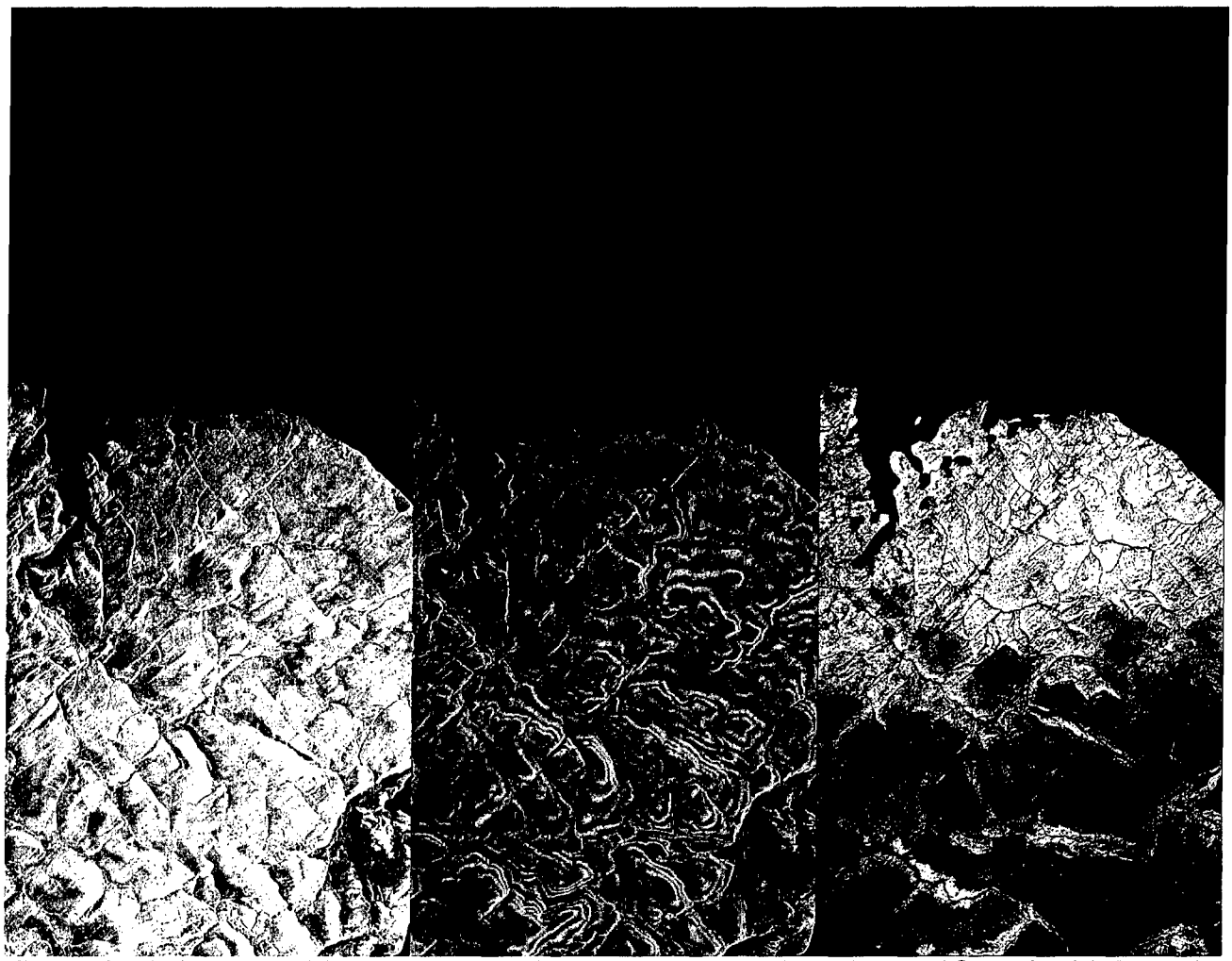

Figure 3: Amplitude, phase (with background amplitude), and coherence images from 8 August – 1 September interferometric data. The image covers an area of approximately 94 km x 38 km. Near range is on the right.

Horizontal mapping accuracy

Four corner reflectors were deployed near Alert. During the spring ground truth mission all four corners were deployed a few hundred meters apart (mostly along the range direction), within a few meters of the southern Sickle point shoreline (see [1] for details). During the summer ground truth mission, two corners were deployed along Sickle Point, as close to their spring position as determined by GPS. Two more corners were deployed along the northern shore of the Upper and Lower Dumbell Lakes. This setup provided for a larger separation of the corners along the radar swath, though still covering only approximately 15% of the swath width. The positions of all of the corner reflectors were measured using C-code GPS receivers, usually more than once. Several problems obscured the corner reflectors from the radar's view. Bears found several of the corners to be irresistible toys. During the spring deployment, windstorms filled some corners with enough compact snow to obscure the radar. Other corners were incorrectly deployed. The number of corner reflectors actually visible in each image is listed in the last column of Table 1.

The surveyed corner reflectors provided clearly identifiable ground control point (GCP) whose location can be identified to within the resolution of the radar and the accuracy of the GPS receiver that surveyed the site. These GCPs were invaluable in determining the geometric accuracy of the system. There are few natural or urban targets that can be reliably used as GCPs. Many GCPs that are readily available to optical systems or in stereoscopy, such as hilltops or road intersections, cannot be identified to sufficient accuracy in radar images. Other targets, such as the oil tanks in Alert, provide a strong radar return but from a focal point that varies with viewing geometry.

The surveyed corner reflectors were then used to assess the horizontal accuracy of the RADARSAT-1 images. Instead of mapping the RADARSAT-1 images to Earth Centred Earth Fixed (ECEF) coordinates and losing image resolution in the process, the GCPs were mapped (or rather reverse mapped) into the radar perspective. This maintains the maximum image resolution and quality. Software was developed for this reverse mapping process. Given the coordinates of a GCP and detailed information about the RADARSAT-1 image (particularly the orbit information), the software will calculate the fractional azimuth line and range pixel (in the radar's slant range perspective, SR) for the GCP. This value can then be compared with the actual image of the corner reflector and an assessment of the horizontal mapping accuracy made.

The result of this comparison for all the visible corner reflector in the spring and summer sets are provided in Table 3. The last two columns of the table provide the offset (in slant range pixels and azimuth lines) between the image location and the surveyed corner reflector (CR). Note Table 2 gives the range pixel and azimuth line spacing in meters for each of the passes. Except for the 30 July pass where the comparatively very large offset may be caused by problems with the orbit data, the offset is within ±4.3 pixels (<31.8 m) and ±3.9 lines (<20.6 m) for the entire data set. There is much greater consistency in the offsets within each individual RADARSAT-1 pass. If any one of the corner reflectors were used to offset the image in range and azimuth, the horizontal accuracy of the radar image would increase significantly. Of the four passes in which all four corner reflectors were visible, the April 4 pass showed the ***largest*** change in the range pixel offset (1.4 pixels or less than 10.4 m). The

April 13 pass showed the ***largest*** change in the azimuth line offset (0.7 azimuth lines or approximately 3.7 m). This implies that if one corner reflector were used to horizontally calibrate the image, the horizontal accuracy would be better than 10.4 m in range and 3.7 m in azimuth.

Table 3: An assessment of RADARSAT-1 horizontal mapping accuracy using surveyed radar corner reflectors

INTERFEROMETRIC PAIR (2002)	NUMBER OF VISIBLE CORNER REFLECTORS (CR)	CR COORDINATES FROM SR IMAGE		CR COORDINATES CALCULATED FROM GPS DATA AND MAPPED TO SR		OFFSET	
		RANGE PIXEL	AZIMUTH LINE	RANGE PIXEL	AZIMUTH LINE	RANGE PIXELS	AZIMUTH LINES
Mar 23	0	N/A	N/A	N/A	N/A	N/A	N/A
Apr 16	1?	1366.1	8141.4	1363.5±0.4	8140.3±0.2	2.6±0.5	0.9±0.3
Apr 13	4	910.1	7824.9	907.0±0.4	7821.0±0.2	3.1±0.5	2.9±0.3
		935.9	7855.7	933.0±0.4	7852.3±1.0	2.9±0.5	3.4±1.1
		970.0	7853.8	966.6±0.5	7850.1±0.4	3.4±0.6	3.7±0.5
		1004.9	7856.1	1002.5±0.7	7852.6±0.8	2.4±0.8	3.5±0.9
May 7	4	910.9	7824.4	909.5±0.4	7826.7±0.2	1.4±0.5	-2.3±0.3
		936.3	7855.1	935.5±0.4	7858.1±1.0	0.8±0.5	-3.0±1.1
		970.6	7853.4	969.1±0.5	7855.8±0.5	1.5±0.6	-2.4±0.6
		1005.3	7855.7	1005.0±0.7	7858.4±0.8	0.3±0.8	-2.7±0.9
Apr 20	?	2944.1	7506.4	2942.3±0.7	7504.1±0.8	1.9±0.8	2.3±0.9
May 14	4	2847.2	7477.0	2844.2±0.4	7478.5±0.2	3.0±0.5	-1.5±0.3
		2874.0	7507.2	2871.0±0.4	7509.3±1.0	3.0±0.5	-2.1±1.1
		2908.3	7504.4	2905.1±0.5	7506.2±0.5	3.2±0.6	-1.8±0.6
		2943.9	7506.1	2941.4±0.7	7507.9±0.8	2.5±0.8	-1.8±0.9
Jul 27	0	N/A	N/A	N/A	N/A	N/A	N/A
Aug 20	0	N/A	N/A	N/A	N/A	N/A	N/A
Jul 30	2?	4221.6	7434.1	4231.0±1.0	9371.3±0.2	9.4±1.1	1937.2±0.3
		4276.6	7362.8	4286.0±1.2	9300.4±0.3	9.4±1.3	1937.2±0.4
Aug 23	0	N/A	N/A	N/A	N/A	N/A	N/A
Aug 4	4	2898.0	5428.2	2893.7±1.1	5431.9±0.4	4.3±1.2	-3.7±0.5
		2967.3	5431.1	2963.8±1.0	5435.0±0.1	3.5±1.1	-3.9±0.2
		3632.4	6121.8	3629.5±0.8	6125.6±0.2	2.9±0.9	-3.8±0.3
		3778.4	6132.9	3775.1±0.3	6136.8±0.2	3.3±0.4	-3.9±0.3
Aug 28	0	N/A	N/A	N/A	N/A	N/A	N/A
Aug 5	2	5219.9	7487.2	5215.9±1.0	7489.9±0.4	4.0±1.2	-2.7±0.5
		5295.5	7477.8	5292.5±0.9	7480.4±0.2	3.0±1.0	-2.6±0.3
Aug 29	0	N/A	N/A	N/A	N/A	N/A	N/A
Aug 8	0	N/A	N/A	N/A	N/A	N/A	N/A
Sep 1	0	N/A	N/A	N/A	N/A	N/A	N/A

We would naturally gain more confidence in these figures if there were more suitable GCPs spread throughout the images, and if such results could be duplicated for other locations around the globe.

The precise source of the horizontal offset in the images, and the change in this offset from pass to pass, has not yet been determined. This offset could be due to a number of factors. These include uncompensated delays in the satellite (causing a range offset), drift in the satellite binary master clock, errors in estimation of the time of the first line in the image, drift in the sampling frequency, errors with the orbit state vectors, image processing errors (including e.g. uncompensated missing lines), among others.

In some geographic locations there may not be any surveyed manmade or natural targets that are clearly visible in the radar imagery and can be used to improve the horizontal registration of the RADARSAT imagery. In such circumstances, a lower resolution map of the area may be useful. When mapped onto the radar image, subtle misregistration between the two may become apparent and consequently used for the horizontal correction.

The ERS satellites offer better horizontal mapping accuracy than that of RADARSAT-1. A recent extensive study of ERS-1/2 has demonstrated the long-term stability of the satellite, with a horizontal mapping accuracy of 10 meters without the use of any GCP [5]. This greater accuracy is due to two main factors. Monitoring the long term stability of delays internal to the satellite, those that can cause horizontal mapping errors, demonstrated that these were stable and measurable. Thanks in large part to the satellite laser ranging system, the position of ERS-1/2 is known to the order of 10 cm to 30 cm [11]. In contrast, the position of RADARSAT-1 is known only to the order of 20 to 100 m [12]. The ERS-1/2 tandem interferometry data offers another great advantage over repeat-pass RDARSAT-1 interferometry data. Whereas RADARSAT-1 (and the upcoming RADARSAT-2) offer a minimal repeat-pass of 24 days, ERS-1/2 tandem pair are separated by only 24 hours. This much shorter temporal interval between interferometric pairs greatly reduces the likelihood of terrain decorrelation due to precipitation.

These advantages of ERS-1/2 come at the expense of resolution. ERS-1/2 has a resolution in ground range of between 21 meters (at far range) and 29 meters (at near range). This compares to a resolution for RADARSAT-1 of between 7.6 and 9.3 meters (depending on which fine resolution mode is used to acquire the data). RADARSAT-2, due to be launched in 2006, will have a best resolution in the ultra-fine mode of approximate ground range and azimuth resolution of 3 m. With the onboard GPS receiver, the real-time position information will have an accuracy of ± 60 meters. This will likely enable more precise horizontal position accuracy than its predecessor, but it will not be as accurate as ERS-1/2.

Coherence filtering

Coherence is a measure of the degree of correlation between two complex data sets. The interferometric coherence magnitude, δ, can be estimated by a sample statistic given by [7]:

$$\delta = \frac{\left| \sum_{i=1}^{L} z_{1i} z_{2i}^{*} \right|}{\sqrt{\sum_{i=1}^{L} |z_{1i}|^2} \sqrt{\sum_{i=1}^{L} |z_{2i}|^2}} \qquad (1)$$

where i is the sample number, L is the number of samples in the coherence window, and z_1 and z_2 are the single look complex (SLC) image of the master and slave.

The number of samples used in the coherence window is an important consideration. Figure 4 shows a plot of the calculated coherence magnitude as a function of the number of samples for relatively high (dashed curve) and low (solid curve) coherence regions of the Alert image. The ***apparent*** coherence varies the most for small values of L. The apparent coherence begins to level off above an L of 40 to 50. Notice also that the apparent coherence for the low coherence regions varies more quickly than then that for high coherence areas.

To find the ***true*** coherence for an area one is either required to use a sufficiently large coherence window or calibrate the coherence as described in [7]. The ***absolute*** coherence has been used in the classification of a variety of targets and features [7,14].

For delineation of shorelines or rivers we rely on land having a high coherence and water, sea ice and rivers having a low coherence. We seek to localize the ***change*** in coherence between the two regions. For this type of application, absolute coherence is not required. Rather, it is necessary to optimize the number of samples used in the coherence window, L, to maximize the descrimination at as high a resolution as possible. A large L will increase the change in coherence between regions of low and high coherence areas. But it will also lower the resolution of the coherence image and blur the delineation between regions of high and low coherence. A small L will help with the delineation, but will lessen the apparent coherence difference between the two regions.

To improve the accuracy of delineating shorelines or rivers we therefore seek to optimize both the ***value*** of L and the ***shape*** of the coherence window. The later is accomplished by the use of appropriate masks. A square coherence window has been the most popular shape for coherence calculations up to now. But it may not be ideal for this application. Li *et al* [9,10] explored a variety of filter shapes and techniques for phase noise reduction, mainly for polarimetry and polarimetric interferometry applications. The coherence filters proposed here for shoreline and river delineation were inspired by them.

Two different types of coherence filters were tested. The most popularly used one is a square window, sliding one (and often more) pixel at a time along range and azimuth, called the ***boxcar*** window or filter. The most common sizes are 3x3 pixels and 5x5 pixels.

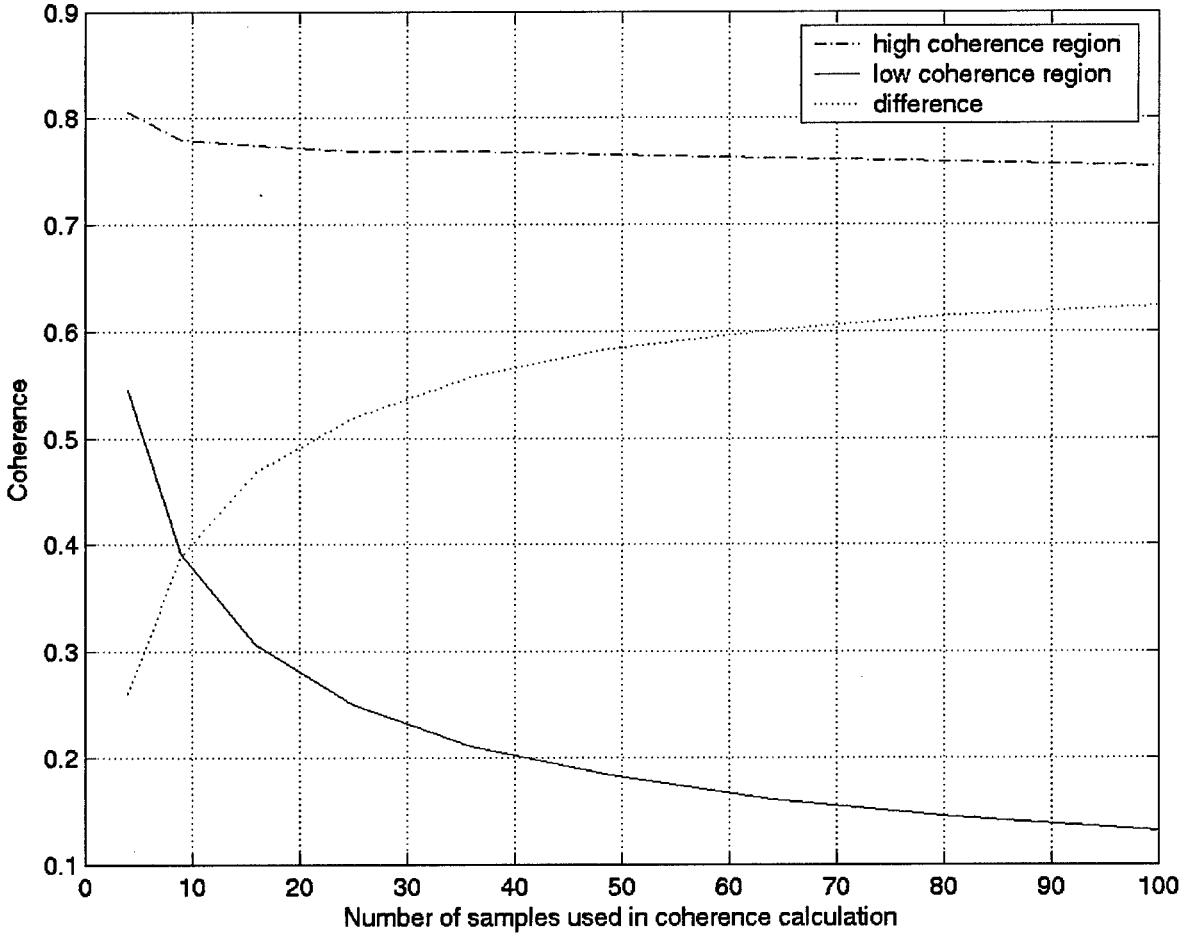

Figure 4: Plot of coherence as a function of number of samples used in the calculation (based on a square window).

The other type of coherence filter tested is a family of filters we will call the three-layer coherence filters. One example of these is the 1x9 three-layer filter shown in Figure 5. The filter is composed of 32 masks, of which only the first 16 are shown. Each mask is composed of 9x9 pixels in three layers. The first step determines the direction of the edge. The coherence (or phase variance) is calculated over the white pixels of all 32 masks. The mask with the highest coherence (or lowest phase noise variance) is selected as the one best aligned with the edge. The final coherence is calculated only over the grey pixels using the selected mask. This value is assigned to the central pixel of the mask. The entire computation then begins anew after shifting the mask relative to the SAR data by one pixel in range or azimuth.

The other filter tested is a larger version of the above. The 1x19 three-layered filter is exactly the same as the 1x9 three-layer filter except that the mask includes 19x19 pixels, and the final coherence is calculated over 19 (rather than just 9) pixels. Referring back to Figure 4, this

larger coherence window size should result in a considerably clearer distinction between the high and low coherence regions. Indeed the tests that follow do indicate that this is the filter of choice for shoreline and river delineation (baring the extra computational cost required).

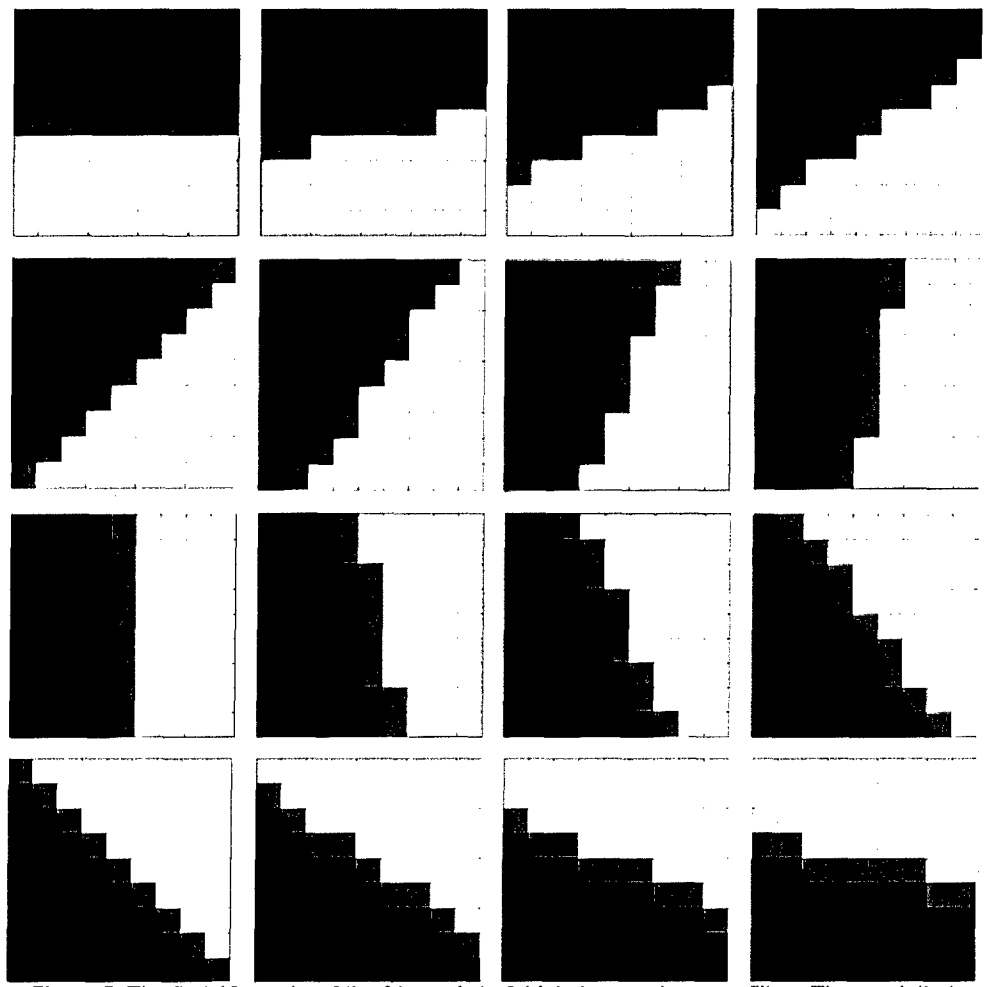

Figure 5: The first 16 masks of the 32 mask 1x 9 triple layer coherence filter. The mask that gives the lowest phase noise (or highest coherence) within the white pixels is chosen. Only the gray pixels are included in the computation of the final coherence.

The three coherence filters described above were tested using idealized shapes imprinted on real data, as well as the Alert RADARSAT-1 interferometric pairs. In the first series of tests, a master SAR image was selected from those acquired over Alert. Its interferometric pair was formed by selectively randomizing the phase of the master image along idealized shapes. Assigning these as an interferometric pair, the coherence was then calculated using the different coherence filters described earlier. The resulting coherence images were then compared with the original idealized shapes.

The first series of idealized shapes is a series of arcs one pixel (in limited areas 2 pixels) thick, shown in the first column of Figure 6. The second column shows the calculated coherence using 3x3 pixels boxcar window, shifted one pixel at a time alternately in range and in

azimuth. The third and fourth columns show the calculated coherence using the 1x9 and 1x19 three-layered filters. Only the 1x19 three-layered filter comes close to maintaining the original shapes – and thickness – of the idealized arc. Filtering (e.g. morphological dilation and erosion operators) may remove most of the extraneous noise.

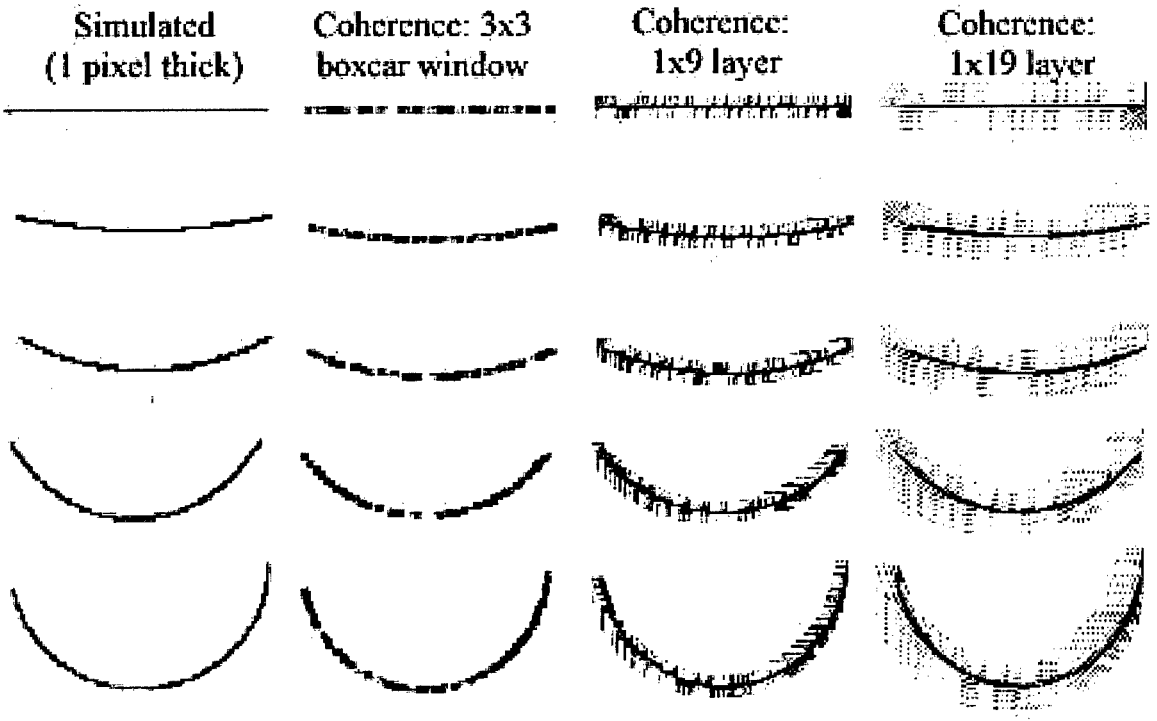

Figure 6: Coherence derived using three different filters and compared with the simulated 'ideal'. To form the interferometric pair, the phase of the 1 September '02 data along simulated curves was randomised and then compared with the original.

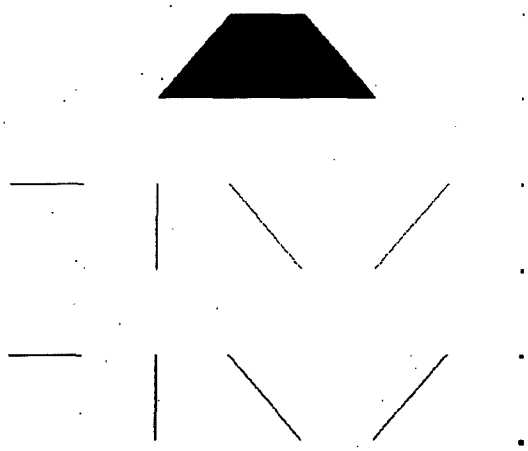

Figure 7: Idealized shapes for coherence tests. They include a trapezoid, four lines one pixel wide, four lines two pixels wide, and a series of 6 dots, 1x1, 1x2, 1x3, 3x4, 4x4, 5x5 pixels.

The second series of idealized shapes is shown in Figure 7. This includes a trapezoid, a set of four lines one pixel wide, a matching set of lines two pixels wide, six dots with widths (from top) 1x1, 1x2, 1x3, 3x4, 4x4, 5x5 pixels.

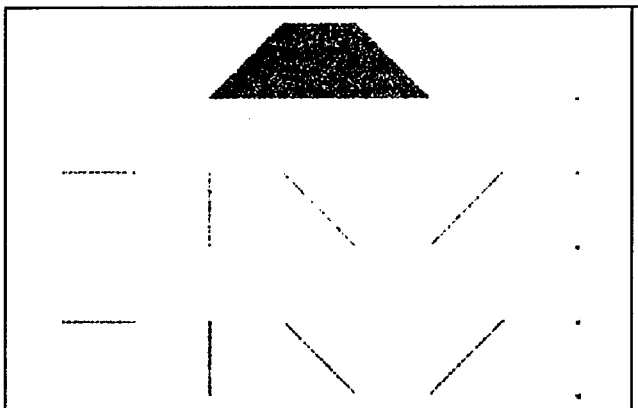

Figure 8: Coherence test with a 3x3 boxcar filter using interferogram with idealized shapes shown in Figure 7.

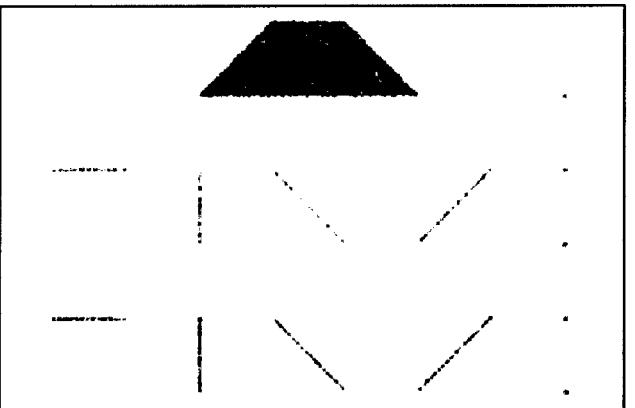

Figure 9: Coherence test with a 5x5 boxcar filter using interferogram with idealized shapes shown in Figure 7.

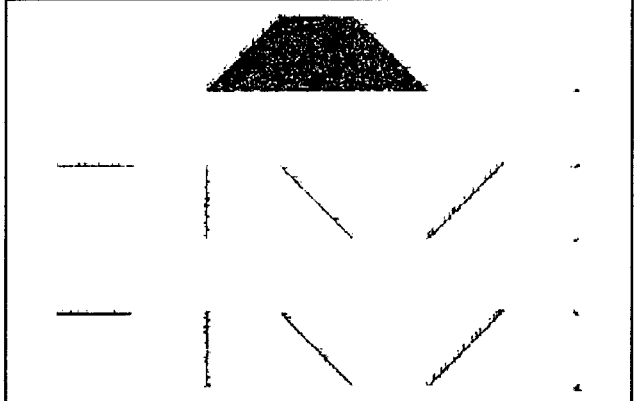

Figure 10: Coherence test with a 1x9 layer filter using interferogram with idleaized shapes shown in Figure 7.

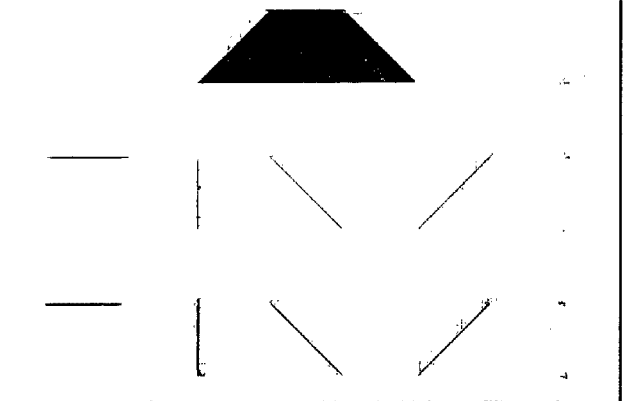

Figure 11: Coherence test with a 1x19 layer filter using interferogram with idealized shapes shown in Figure 7.

These idealized shapes form a more stringent test of the coherence filters. They bring out the strengths and weakness of each filter. The calculated coherence using a 3x3 and 5x5 boxcar filters are shown in Figure 8 and Figure 9 respectively. The calculated coherence using the 1x9 and 1x19 three-layered filters are shown in Figure 10 and Figure 11 respectively. Although the boxcar filters are not as faithful in reproducing the thin lines or as accurate in delineating the flat edges of the trapezoid, they are better at detecting the series of dots on the right side of each image. They are also more computationally efficient. The difference between the 3x3 and 5x5 boxcar filters is subtle. Because of the larger number of elements in the coherence sum, the contrast between the high and low coherence regions is slightly better with the 5x5 boxcar filter.

The 1x19 three-layered filter is the best at reproducing the thin lines and the edges of the trapezoid. It even reproduces the corners of the trapezoid quite faithfully. It does not reproduce the dots well, and therefore would not be suitable for detecting very small targets (small in comparison with the resolution of the system). Computationally it is also more intensive than the boxcar filter. The only advantage to the 1x9 three-layered filter is in this respect. It is slightly less computationally intensive than the 1x19 version, but more than the boxcar filters.

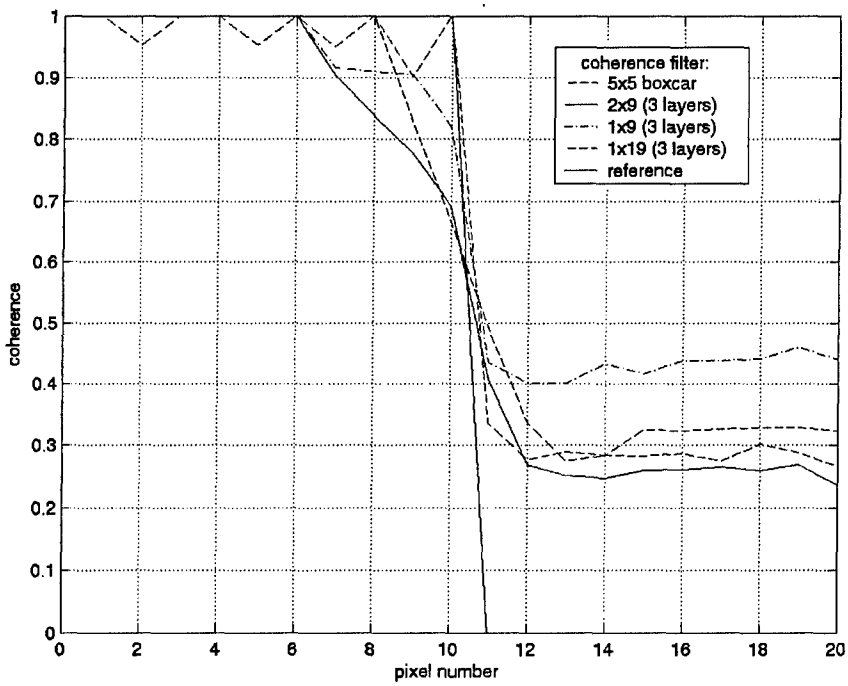

Figure 12: Plot of the coherence derived using 4 different filters across a simulated shoreline.

The long side of the trapezoid is used to simulate an idealized shoreline, and test how well the various coherence filters perform in comparison. Figure 12 shows a plot of the coherence across the long sides of the trapezoid of Figure 7. The solid black line represents the idealized shoreline, with an abrupt one-pixel change from land (with a coherence of 1) to sea (with a coherence of 0). The other lines represent the similar plot across the filtered trapezoids. A 2x9 three-layered filter was included for comparison. The 1x19 three-layered filter again performs best overall. It follows the idealized shoreline most closely and offers a relatively large change in coherence between the two regions. The 5x5 boxcar filter and the 2x9 three layered filter perform the worst. The calculated deviation from the location of the idealized shoreline based on four of the coherence filters is listed in Table 4.

Table 4 Calculated deviation from the location of an idealized shoreline based on four of the coherence filters.

SIMULATED RIVER ONE PIXEL WIDE	IDEAL	1X19 FILTER	2X19 FILTER	3X3 BOXCAR FILTER	5X5 BOXCAR
MEAN (PIXELS)	0	0.01	0.18	0.18	0.71
STANDARD DEVIATION (PIXELS)	0	0.10	0.39	0.77	0.79

In the last simulation, a river is idealized as a decorrelated line one pixel wide. Figure 13 shows a plot of the coherence across one of the lines shown in Figure 7. The solid black line

represents a cut across the idealized river. The other lines represent a similar cut across the filtered line. Using the 5x5 boxcar filter, the idealized decorrelated line is all but lost. By contrast the 1x9 and 1x19 three layered filter perform very well (with the later holding a slight edge). The calculated width of the simulated river based on four of the coherence filters is listed in Table 5.

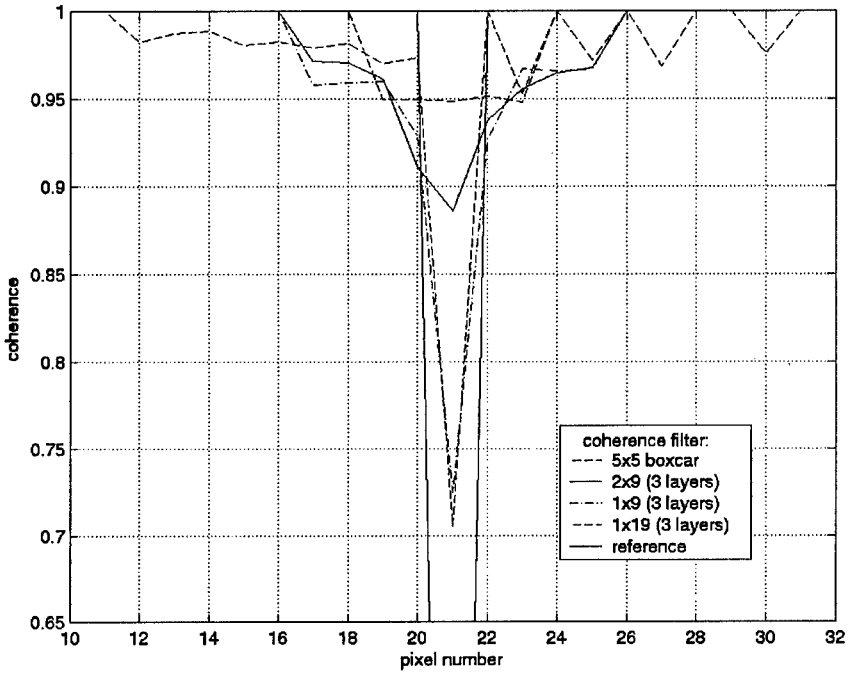

Figure 13: Plot of the coherence derived using 4 different filters across a completely decorrelated line one pixel wide.

Table 5 Calculated width of a simulated river based on four of the coherence filters.

SIMULATED RIVER ONE PIXEL WIDE	IDEAL	1X19 FILTER	2X19 FILTER	3X3 BOXCAR FILTER	5X5 BOXCAR
MEAN (PIXELS)	1	1.1	2.2	2.1	3.6
STANDARD DEVIATION (PIXELS)	0	0.6	1.7	1.3	2.1

These tests demonstrate the strengths and weakness of each filter. The 1x19 three layered filter is better for the idealized shorelines and rivers. The 5x5 boxcar filter is better for small isolated areas, and is computationally much more efficient. To determine how they compare with real data, these two filters were tested using a portion of the 8 August/1 September interferometric dataset. Figure 14 shows the coherence as calculated using the 1x19 three layered filter. Figure 15 shows the coherence as calculated using the 5x5 boxcar filter. This

represents an area approximately 6.7 km x 10 km, with near range along the right size of the image in this descending pass.

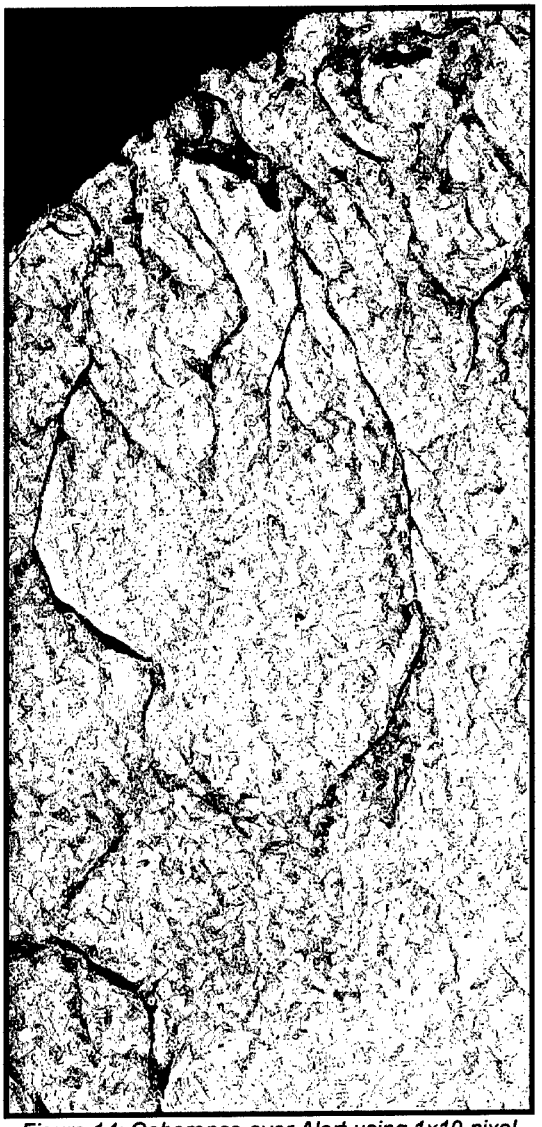

Figure 14: Coherence over Alert using 1x19 pixel layer with data from 8 August/1 September 2002 pair. This represents an area approximately 6.7 km x 10 km, with near range along the right size of the image in this descending pass.

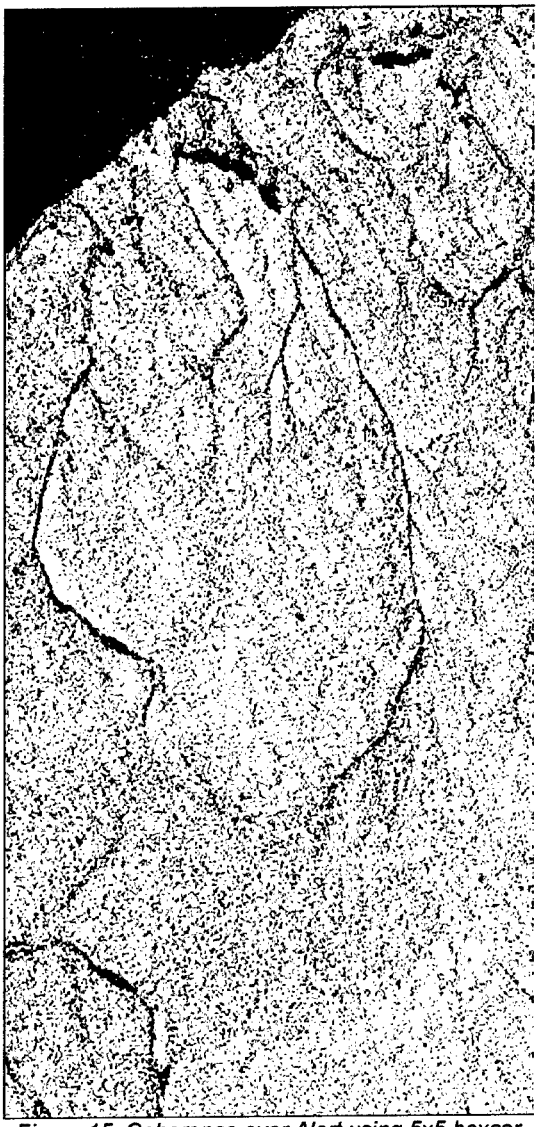

Figure 15: Coherence over Alert using 5x5 boxcar filter with data from 8 August/1 Septempber 2002 pair. This represents an area approximately 6.7 km x 10 km, with near range along the right size of the image in this descending pass.

Target and feature detection

The extent of the ground truth obtained permitted us to expand the original experiment design to include a study of target and feature detection. We attempt to address the question; how well do RADARSAT-1 magnitude and phase data compare in target and feature detection, particularly in an arctic environment.

A complete list of the targets and features surveyed using GPS and photographed during the ground truthing is listed in [1]. Many of these targets were then mapped into radar perspective using these GPS measurements. Their horizontal position, now given in slant range pixels and azimuth lines, were calibrated using the surveyed corner reflectors in the scene. The targets were finally located on the radar image permitting a direct assessment of how well the radar image perceives the target. Mapping the targets into the radar perspective permitted preservation of the maximum resolution of the radar images. It is also computationally ***much*** more efficient than the alternative.

Figure 16 is a magnitude image of the central portion of Alert from the 4 August data set with the mapped target indicated by green circles. Among the surveyed targets that are clearly visible (and well mapped) are the eight fuel tanks, the Spinnaker building and the met station shack. The eight oil tanks are metal with metal ladders and other structures on the side and top. The Spinnaker building is one of the brightest targets in the radar scene, not doubt due to its corrugated metal walls and roof that offer a strong target for the radar. The met station is also a metal building with a corrugated metal roof with a couple of metal towers nearby. Many other buildings in Alert that were not surveyed are also clearly visible in the radar images. Most of these are metal in structure, some with some fibreglass components. The other surveyed targets, such as the two piles of crushed stone, the met station sensors, and the antenna site, are not detectable.

A more complete list of surveyed targets and their visibility in the magnitude or phase images is provided in Table 6. The visibility of the target is classified in decreasing order of their visibility in the images as "stong", "yes", "hint", or "no". Because of the low resolution of the radar, coherence did not offer any advantages for detecting small individual target, given the low resolution of RADARSAT-1 and was therefore not included in the assessment. Rather than discussing the targets that were detectable, it is actually more informative to focus on those that were undetectable, or barely detectable. The three airplane crash sites are not clearly detectable either in the snow covered spring images or in the snow free summer images. This includes the 1991 Hercules, the Lancaster and DC4 crash sites. This may be due to the combination of the insufficient resolution of the fine mode of the image and the particular incidence angle used to image the target. None of the surveyed stone piles and stone monuments were detectable. Several of the smaller shacks, such as the pump station building (including transformer and generator), the Bench Mark tide shack and the GPS antenna tide shack, are weakly detectable. These are wooden, metal, and fibreglass structures.

Compacted snow may be partly responsible for some of the low radar returns. If deployed correctly, radar corner reflectors reflect a very strong signal back to the radar; a signal that is clearly visible in the imagery. On several occasions snow that was heavily compacted into the

corner reflector by the wind may have been sufficient to effectively obscure the reflector from the radar.

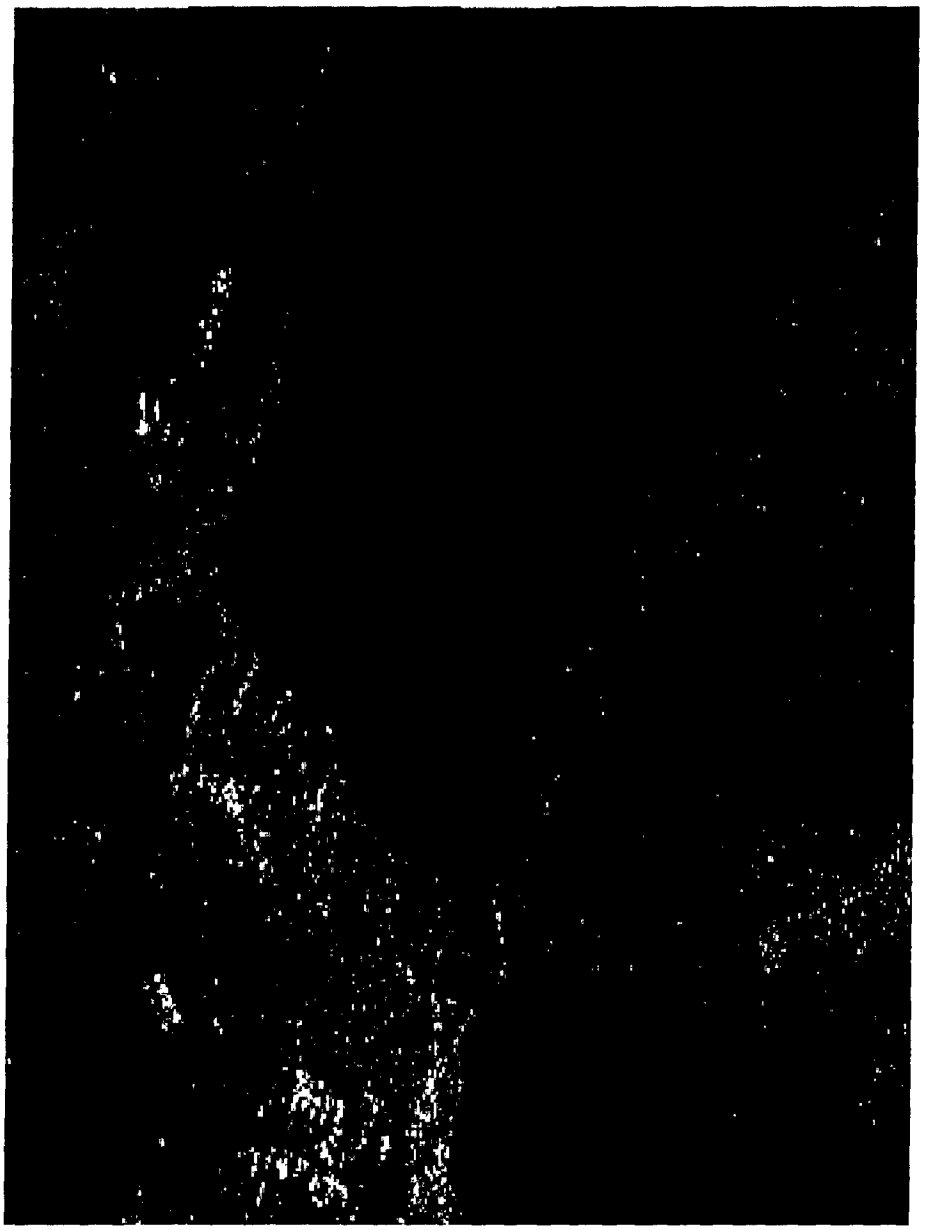

Figure 16: 4 August 2002 amplitude image (in grey) compared with several ground control points (green circles). The average of four corner reflectors with GPS reference was used to reference the radar image, adjusting the overall scene by 3.5 pixels in range and –3.8 lines in azimuth. On the right: Antenna site. On the left from bottom: Alert HQ, ID #64, 8 fuel tanks, crushed stone pile (ID #78), crushed stone pile (ID #77), ID #76, Spinnaker building, met station sensors, met station shack.

Table 6: Detection of various targets in RADARSAT-1 images

WAY POINT DESCRIPTION & ID#	VISIBLE TARGETS	
	RADAR MAGNITUDE 4 AUG'03	PHASE & MAGNITUDE 8 AUG '03
Fuel Tank #1(68)	Strong	Strong
Fuel Tank #2 (69)	Strong	Strong
Fuel Tank #3 (70)	Strong	Strong
Fuel Tank #4 (71)	Strong	Strong
Fuel Tank #5 (72)	Strong	Strong
Fuel Tank #6 (73)	Strong	Strong
Fuel Tank #7 (74)	Strong	Strong
Fuel Tank #8 (75)	Strong	Strong
Crushed Stone Pile (77)	No	No
Crushed Stone Pile (78)	No	No
Pump Stn Wood Bldg (79)	No	No
Pump Stn Transformer (80)	No	No
Pump Stn Generator (81)	Yes	Yes
Pickup Structure (82)	Yes	Yes
Met Stn Sensors (83)	No	No
Met Stn Shack (84)	Yes	Yes
HydroGraphic BM (85)	No	No
Cnr-Seal Upper Dumbell (86)	Strong	NA
Metal Bldg Upper Dumbell (87)	No	No
Cnr-Sandpiper Lower Dumbell (88)	Strong	NA
Cnr Caribou Sickle Point (93)	Strong	NA
Cnr Bear Toy Sickle Pt (94)	Strong	NA
Cnr Caribou Sickle Point (98)	Strong	NA
Cnr Bear Toy Sickle Point (99)	Strong	NA
Cnr-Sandpiper Lower Dumbell (102)	Strong	NA
Cnr-Seal Upper Dumbell (103)	Strong	NA
Ice Cave (Tunnel) (105)	No	No
Cairn NW White Pond (106)	Yes	No
Love Shack Kirk Lake (107)	No	No
Antenna East of Narrows (108)	No	No
Cnr Caribou Sickle Point (109)	Strong	NA
Cnr Bear Toy Sickle Point (110)	Strong	NA
Cnr-Sandpiper Lower Dumbell (111)	Strong	NA
Cnr-Seal Upper Dumbell (112)	Strong	NA
Bench Mark Tide Shack (113)	No	Hint
GPS Antenna Tide Shack (114)	No	No

Perry Winter over Quarters (115)	No	No
Tin Can Deposit (116)	No	No
Barrel Hoops (117)	No	No
Mel Christian Petersen May 1876 (118)	No	No
Cairn Two Trees (119)	No	No
Cairn White Cross "R" (120)	No	No
3 (Rock) Foundations on Beach (121)	No	No
Ross & Marvin 10April 1909 (122)	No	No
Cairn above Jolliffe Bay	No	No
Lancaster Crash Site	No	No
DC-4 Crash Site Edge of Runway	No	No
Monument 31 July 1950 Air Crash	Poor	Hint
ALERT HQ	Strong	Strong
BEARTOY Corner	Strong	NA
CARIBOU Corner	Strong	NA
DUMBELL Corner	Strong	NA
RAVINE Corner	Strong	NA
SANDPIP Corner	Strong	NA
SEAL Corner	Strong	NA
SICKLE Corner	Strong	NA
CREEK	Yes	Yes
CRN SE JFB	No	No
DC4 CRASH	No	No
ICE CAVE Tunnel	No	No
LANCASTER Site	No	No
Monument 1950 Alert	No	No
Spinnaker Bldg	Strong	Strong
Hercules 1991 crash site	No	No
Oopic Island (162) – top centre	Yes	Yes

Shoreline, riverbed, and trail detection

Ascertaining the variety of shorelines, riverbeds, and roads that can be detected with RADARSAT-1 is of greater interest in this study. The ground truthing that occurred in the spring and summer of 2002 included GPS measurement of shorelines, and a variety of different roads. These are delineated in blue in Figure 1. They are listed in the second column of Table 7, and described in more detail in [1]. The procedure outlined in the previous section for mapping the surveyed targets into radar perspective was followed for the roads as well. They were then superimposed onto the magnitude, phase, and coherence images interferometric pair (following horizontal shifting of the images based on the surveyed corner reflectors). A visual subjective assessment was then made to ascertain how clearly the roads are discriminated in each of these images. The result of this assessment for each of the surveyed roads using the spring and summer pair that appear in Figure 2 and Figure 3 is shown in Table 7.

Several conclusions can be drawn from this study. Coastlines and shorelines of lakes were much more readily detectable in the coherence image than in the radar magnitude, thereby lending itself much more readily to automated delineation. Rivers and riverbeds were also much more easily detected in the coherence image and therefore their delineation would be much easier to automate. Roads, on the other hand, were often not clearly detectable, either in the magnitude, phase, or coherence images. The resolution of RADARSAT-1 is clearly a limitation, but optimizing the incidence angle for the target in question may help.

Consistency in the detection of shorelines using coherence is a very important issue. In an attempt to address this, an understanding of the phenomena that causes change in coherence is needed. Let us consider the summer and winter seasons separately. During the summer months most of the ice on the rivers, and lakes, as well as the sea ice have melted. The ground is generally rocky, free from tall vegetation and, thanks to the sparse rainfall during the summer of '02 [1], also dry. The large change in water content between the dry shores or riverbanks versus the water results in the loss of coherence [4]. Several factors can cause loss of coherence on the land and degradation of the coherence. These include rain causing high moisture content of the ground, large trees whose footprint changes from pass to pass at C-band, tropospheric effects [4, 8], and ionospheric effects (which are more problematic at L-band) [2].

During the winter or snow-covered seasons the situation is more complex. Several mechanisms are responsible for the variations in coherence. Wind induced snow compaction and variation in the snow depth is probably responsible for the loss of coherence (or decorrelation) in riverbeds and steep valleys. Snow compacted into one of the corner reflectors during our experiments caused it to be completely obscured from the radar. Open terrain is windswept and therefore experiences less variation in snow accumulation providing for better coherence.

Table 7: Visible shorelines, riverbeds and roads

NO	SHORELINE/TRAIL	VISIBLE SHORELINES, RIVERBEDS & ROADS

	REFERENCE NAME	20 APR/14 MAY '03			8 AUG/1 SEP '03		
		MAG	PHASE & MAG	COH	MAG	PHASE & MAG	COH.
1	AirStrip29Jul	Yes	Yes	Parts	Yes	Yes	Yes
2	AirStrip05Aug	Yes	Yes	Parts	Yes	Yes	Yes
3	ColonBayLDBCreek	Parts	Yes	Parts; low coherence	From Layover; Coast	Yes	Yes
4	DumbellWaterLine	Hints in part	Hints in parts	No	Hints in parts	Hints in part	No
5	FloebergBeachTrip	Mainly creeks & riverbeds	Mainly creeks & riverbeds	Part along Riverbed & coast	Riverbed only	Mainly creeks & riverbeds	Creek & Riverbed
6	HilgardHike29Jul	No	No	No	No	No	No
7	HQtoSpinkr24Jul	Mostly	Mostly	Mostly	No	Portions	No
8	JP8Pipeline	Hints	Hints	Hints	No	No	No
9	KirkCreektoHQ	Hints	Creeks + hints	Parts	No	Creeks + hints	Bits & hints
10	KirkLakeIceCave	Hints: Creeks & Riverbeds	Creeks & Riverbeds	Creeks & Riverbeds	No	Creeks & Riverbeds	Bits & hints
11	LDBCreekColonBay	Parts vague	Yes	Mostly	Yes	Yes	§Yes
12	LDBCreekWest	Yes	Yes	Mostly	Yes	Yes	Yes
13	LoDumbellExitA	Yes, vague	Yes	Mostly	Yes	Yes	Yes
14	LowerDumbellWest	Yes, vague	Mostly	Yes	Yes	Yes	Yes
15	RoadTankstoSpinkr	Yes	Yes	Yes	Hints	Good hints	Hints
16	SicklePointTrack	N part obscured by ice	Yes	Yes, 1-5 pixel gap	Short gap	Yes with short gap	Yes
17	UpperDumbellLake	Yes but vague	Mostly	Mostly	Yes	Yes	With deviations
18	UpperDumbellLaketoHQ	Vague shoreline and trail	Shoreline only	Shoreline only	Shoreline only	Shoreline, hints of trail to HQ	Part of trail to HQ
19	WilliamIsA	Slightly obscured by ice	Yes, 1-10 pixel gap	Yes, 1-10 pixel gap	Some gaps	Yes, but smaller	Yes

C-band radar has been observed to penetrate fresh water ice to a depth of 12 to 35 m [6]. The ice thickness on local lakes typically increases steadily through the winter while the snow depth varies. During the winter of 2002/03 for example, the ice thickness on Dumbell Lake reached 140 cm in February, while snow depth varied between 5 and 27 cm [15]. As a result, the scattering mechanism from fresh water lake ice is largely due to volume scattering. This contrasts with the predominantly surface scattering of the surrounding, wind swept, terrain. With a proper choice of baseline [4], this difference in the predominant scattering mechanism results in a measurable change in coherence [6,13], thereby outlining the lakes.

The frozen sea is displaced vertically by the tide, causing the level of the sea ice to vary between 10 cm and 80 cm [4]. Large blocks of ice are beached along the some of the shores (see photographs in [4]). During the winter of 2002/03 the sea ice thickness in Parr Inlet was observed to increase gradually reaching approximately 180 cm in March, with snow depth varying through the course of the winter between 5 and 31 cm [15]. The constantly varying level of the sea ice against the land causes a thin sheer region to develop between the two. In earlier work around Bathurst Island this thin, sheer region was clearly visible as a thin ribbon of low coherence, and contrasted well with the relatively high coherence of the land and the stable mass of sea ice, thereby clearly outline the coastline [4]. During this trial, the amplitude images clearly indicate that the northern portion of the sea ice was unstable between acquisitions, resulting in the low coherence observed for that region. The land fast portion of the sea ice is north and adjacent to Alert. Volume decorrelation is likely the cause of the loss of coherence. Its coherence is low, although not as low as the unstable sea ice to its north [16].

Coastline delineation accuracy

Comparing the position of the shoreline as derived using interferometric coherence with the GPS data provides a measure of accuracy. As mentioned earlier, the GPS data was converted from latitude, longitude and height measurement into the radar's range and azimuth perspective. The data were then horizontally shifted using the surveyed corner reflectors, and mapped onto the coherence image.

The delineation of the shoreline using coherence is a similar process to generating contour intervals from elevation data. In this study interactive Matlab contouring routines in combination with a photo editor were used to generate and filter the contour of the shoreline. The resulting contour is unrealistically curved in areas, but will suffice for the immediate purposes of this comparison. More sophisticated and automated programs are clearly necessary, but are beyond the scope of this study. Software that the mapping industry use for contour generation may very prove suitable to this task, but were unavailable to this authors.

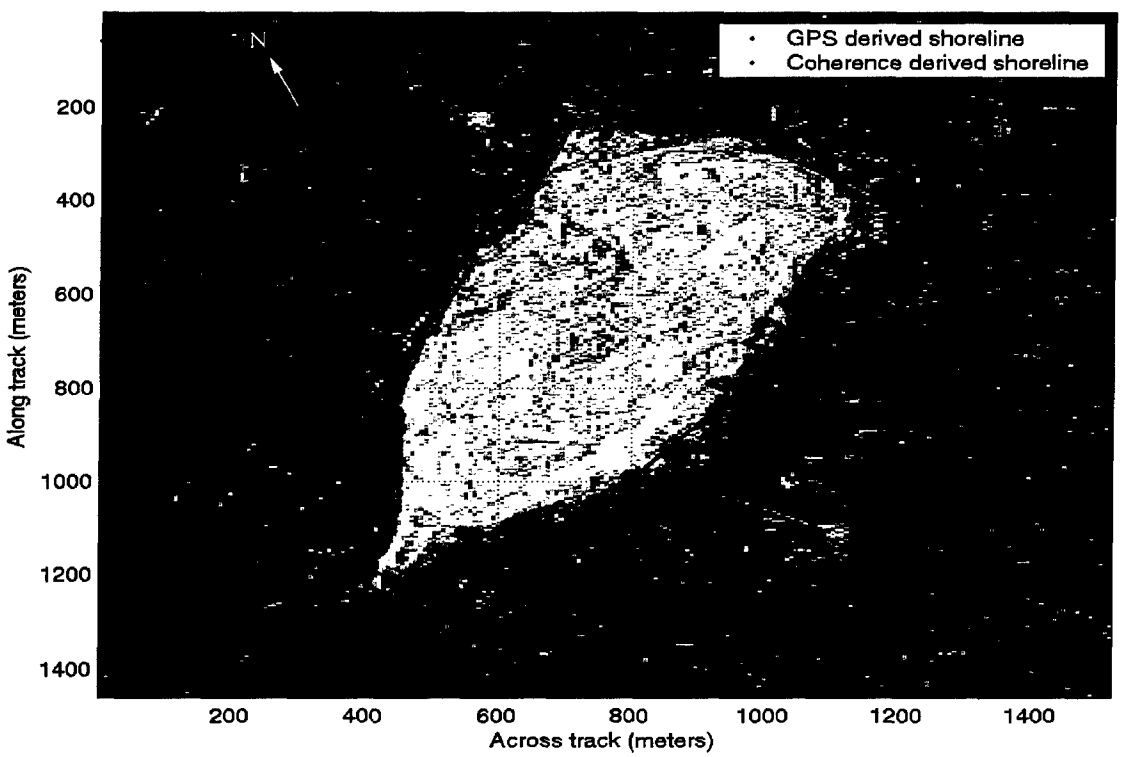

Figure 17: Williams Island shoreline derivation comparison (8 August/1 September 2002 InSAR data). GPS data were collected in April 2002 with snow covering the entire area.

Three different coastlines where selected from the Alert experimental dataset for this accuracy assessment. The first comparison, shown in Figure 17, is Williams Island. The GPS and coherence derived coastlines, shown in red and blue respectively, are mapped onto the coherence image. The GPS data were acquired in spring with both the land and sea covered

in snow. The location of the coastline therefore had to be estimated by the operators of the GPS receiver, adding to the uncertainly of the GPS derived coastline. The coherence data were derived from the 8 August/1 September data pair using the 1x19 three layered coherence filter. The deviation between the two coastline estimates is shown Table 8. The mean deviation is 7.7 m and the standard deviation is 7.8 m. The Linear error perpendicular to the GPS measured shoreline at 90% confidence level (LE90) is 13.2m. Based on the EPE (Estimated Position Error) reported by the GPS receiver, the GPS measurements are considered accurate to 3 to 4 m.

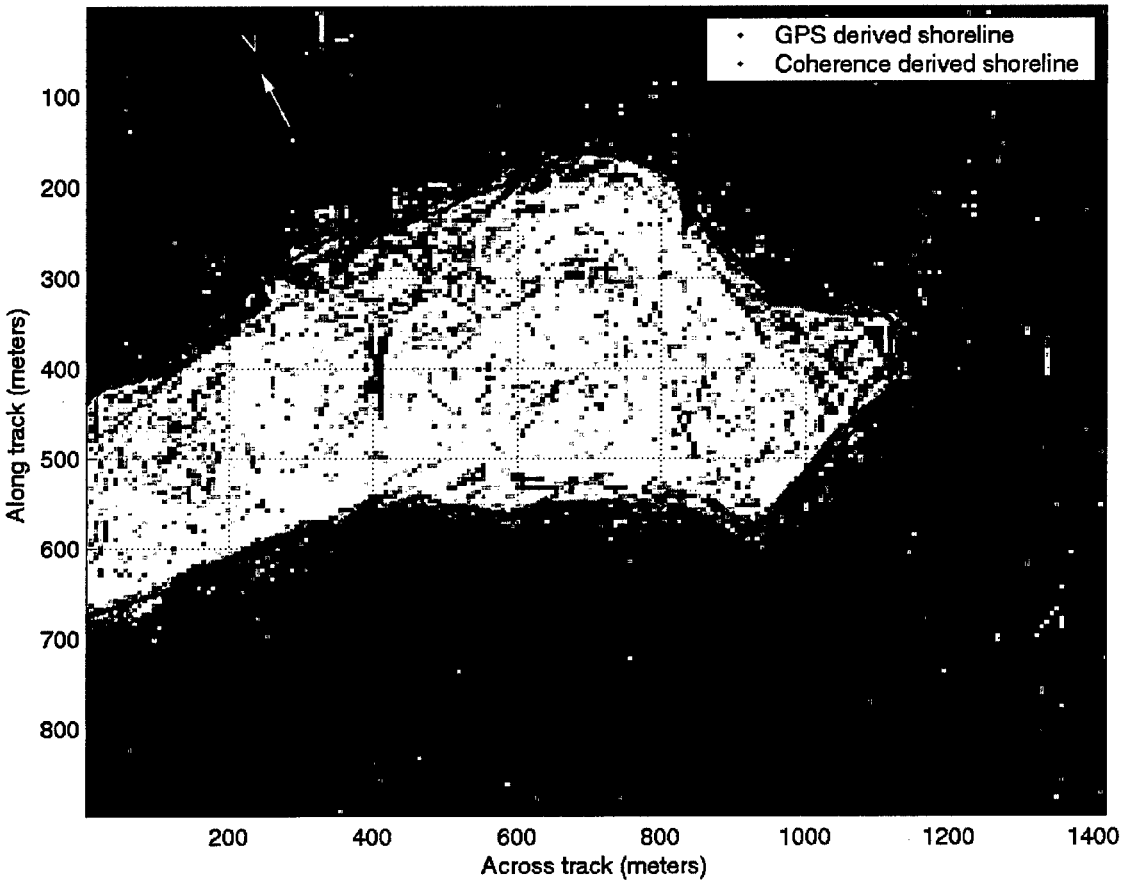

Figure 18: Sickle Point shoreline derivation comparison (8 August/1 September 2002 InSAR data). GPS data were collected at low tide on 30 July 2002.

The second coastline derivation comparison is Sickle Point, and is shown in Figure 18. A winter and summer aerial photograph of the peninsula is shown in Figure 19. Note the presence of sea ice, even in the summer scene. This GPS data were collected at low tide on 30 July 2002. The GPS operator followed the coastline with one foot in the water and the other on land. The deviation between the two coastline estimates is also listed in Table 8. The mean deviation is 6.9 m and the standard deviation is 5.3 m. The Linear error perpendicular to the GPS measured shoreline at 90% confidence level (LE90) is 9.0 m. Once again the GPS measurement was accurate to 3-4 m.

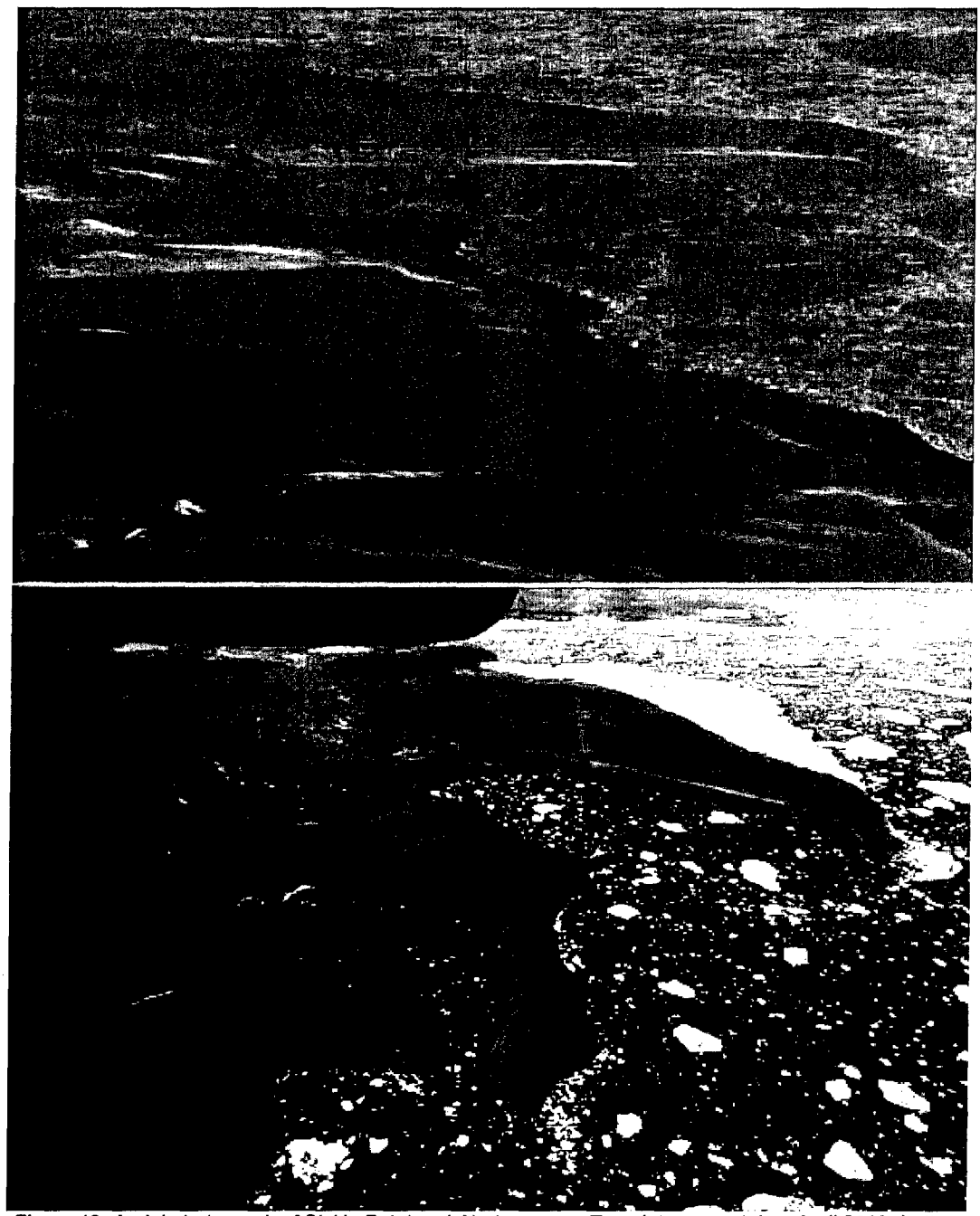

Figure 19: Aerial photograph of Sickle Point and Alert runway. Top picture was taken April 2002, bottom one was taken July 2002. (courtesy of J. Lang)

The last shoreline compared is that of Upper Dumbell Lake, Figure 20. Note that the small island near the southern shores of the lake was not well rendered by the 1x19 coherence filter.

As mentioned in a previous section, small features are better rendered using the standard boxcar coherence filter.

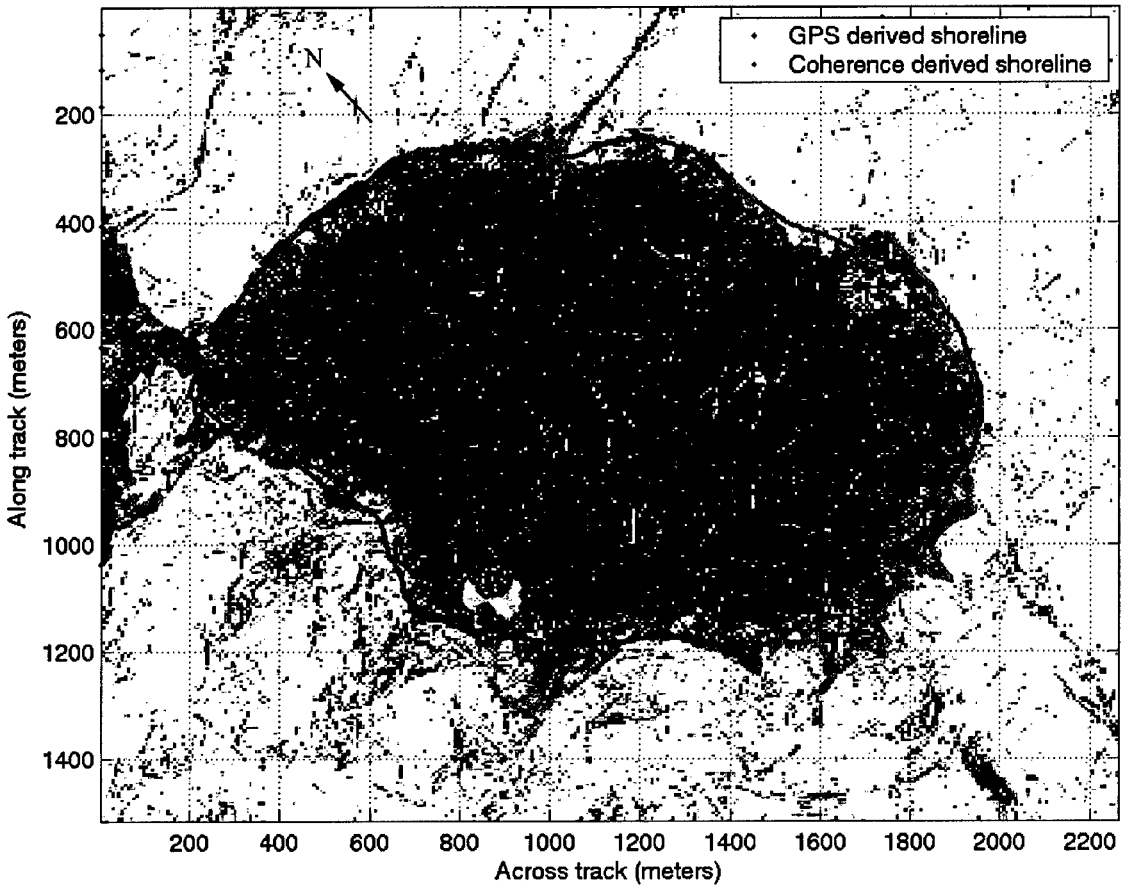

Figure 20: Upper Dumbell Lake shoreline derivation comparison (8 August/1 September 2002 InSAR data)

Table 8: Difference in shoreline delineation using 1x19 three layered coherence versus GPS survey. Uncertainty in GPS is 3 to 4 m. Williams Island was surveyed in spring 2002 with both the ground and sea ice covered with snow and the location of the shoreline estimated visually.

Shoreline	Mean (m)	STD (m)	LE90 (m)[1]
Williams Island	7.7	7.8	13.2
Sickle Point	6.9	5.3	9.0

The difference between the GPS shoreline track and the coherence generated shoreline can be attributed to errors both with the GPS and the coherence measurement. Only a single GPS receiver was used in these surveys (i.e. not in differential GPS mode). The Estimated Position Error (EPE) reported by the GPS receiver was between 3 to 4 m. Furthermore, GPS track measurements of the Upper Dumbell Lake and Williams Island shorelines were carried out in winter with both the ground and sea ice covered with snow, thereby obscuring the exact

[1] Linear error perpendicular to GPS measured shoreline at 90% confidence level.

position of the shoreline. Various stages of the coherence shoreline measurement can cause errors in shoreline delineation. During the colder months, beached icebergs add to the coherence shoreline uncertainty. Thick snow cover near the shoreline can cause attenuation of the radar signal, therefore causing a loss of coherence and obscuring the exact location of the shoreline. During the warmer months, soil moisture near the shoreline can cause attenuation of the radar signal. Therefore, depending of the type of earth at the shore, the coherence can be delineating the interface between dry and moist soil rather than the sea-land interface. Errors in generating the contour lines from the coherence mask was a more serious problem in this study due to the rudimentary contour masking employed. In addition, the coherence mask used is good at reproducing quasi-linear features in the coherence, but may distort small round islands.

Conclusion

This study demonstrated that repeat-pass RADARSAT-1 interferometry is potentially a valuable and accurate technology for coastline and riverbed delineation and mapping in Arctic environments. Decorrelation effects, normally significant over the 24 days that separate a RADARSAT-1 interferometric pair, are minimized in Arctic environments. Shorelines and riverbeds are delineated by a sharp change in coherence.

The methodology for accurate shoreline delineation was developed and tested using ground truth and repeat-pass RADARSAT-1 interferometric data of Alert, Nunavut. In total, eight RADARSAT-1 pairs were collected, three in the spring and five in the summer of 2002. While several of the passes proved to have low coherence due to local weather conditions, two pairs of passes (one in each season) proved to have a very good coherence over the test area.

The methodology included two key steps. The first step was to improve the horizontal mapping accuracy of RADARSAT-1. In this study, up to four surveyed corner reflectors were deployed near Alert and used to assess the horizontal mapping accuracy of seven of the RADARSAT-1 scenes. Horizontal position errors of up to five range pixels (approximately 35 meters) and five azimuth lines (approximately 25 meters) were observed. Much greater consistency was observed within each passes than between the various passes. As a result it was demonstrated that using a single ground control point (GCP) in a scene improved geometric accuracy of that scene to better than 1.4 slant-range pixels (approximately 10.5 meters) and 0.7 azimuth lines (or 3.7 meters). If a manmade or natural GCP, suitable for radar imagery, is not available for reference, a digital elevation map of the site may help instead.

Long term monitoring of ERS-1/2 tandem interferometry data demonstrated that it consistently achieves 10 meter horizontal mapping accuracy. The 24 hours that form the temporal separation of the tandem pair (compared with a minimum temporal separation of 24 days for RADARSAT-1/2) is also very important and will significantly reduce coherence loss over land from precipitation. These important advantages of the ERS satellites are offset by its lower resolution. Compared with the ground range and azimuth resolution of the fine-beam mode of RADARSAT-1 of approximately 9 x 9 meters respectively, ERS-1/2 has a resolution of 23 x 6 meters respectively. RADARSAT-2 will have a resolution of approximately 3 x 3 meters in the ultra-fine mode, and perhaps have a slightly better horizontal mapping accuracy than RADARSAT-1 (but still worse than the ERS or ENVISAT satellites).

The second key step maximizing shoreline delineation was to design a coherence filter specifically for accurate delineation of quasi-linear changes in the coherence. The delineation accuracy of the filter was tested using both simulated data and RADARSAT-1 interferometric pairs collected over Alert, Nunavut and determined to be a significant improvement over the commonly used coherence filters.

Using this methodology, the shoreline was derived using coherence at several locations around Alert and compared with in situ GPS track measurements. The mean difference (and standard deviation) between the two shorelines was less than 8 meters. Part of this difference is due to uncertainty with the GPS measurement (on the order of 3-4 meters) and partly errors in the coherence delineation.

Assessment of the horizontal mapping accuracy of RADARSAT-1 should be expanded to include tests over larger test sites, as well as long term monitoring of the stability of the system, similar to the in-depth study carried out with the ERS satellites. A deeper understanding of the real source of these changing across-track and along-track delays may help reduce the need for such a geometric calibration procedure. In addition, more accurate and automated contouring programs and contour filtering programs are needed to improve the accuracy and automation of delineation of the shoreline from the coherence images.

The amplitude, phase, and coherence of RADARSAT-1 proved less reliable in detection of small targets, features, and roads such as three airplane crash sites, and fairly large stone monuments. With its improved resolution, RADARSAT-2 may prove better at detecting such features. By comparison, metal buildings, especially those with corrugated sides and riverbeds were clearly visible.

References

1. K.E. Mattar, L. Gallop, J. Lang. (2002). "Alert 2002 ground truth missions for Arctic shoreline delineation and feature extraction," (DRDC Ottawa TM 2002-147), Defence R&D Canada – Ottawa.

2. K.E. Mattar & A.L. Gray, "Reducing ionospheric electron density errors in satellite radar interferometry applications," *Can. J. Remote sensing*, Vol. 28, No. 4, pp. 593-600, 2002.

3. M. Yeremy, A. Beaudoin, J.D. Beaudoin, G.M. Walter. (2001). "Global shoreline mapping from an airborne polarimetric SAR: assessment for RADARSAT 2 polarimetric mode", (DREO TR 2001-056), Defence Research Establishment Ottawa.

4. K.E. Mattar, M. Buchheit, & A. Beaudoin. (2001). "Shoreline mapping using interferometric SAR", (DREO TR 2001-078), Defence Research Establishment Ottawa.

5. J.J. Mohr and S.N. Madsen, "Geometric Calibration of ERS Satellite SAR Images", *IEEE Transactions on Geoscience and Remote Sensing*, Vol. 39, No., 4, pp. 842-840, April 2001.

6. E.W. Hoen and H.A. Zebker, "Penetration Depths Inferred from Interferometric Volume Decorrelation Observed over the Greenland Ice Sheet", *IEEE Transactions on Geoscience and Remote Sensing*, Vol. 38, No. 6, pp. 2571-2581, November 2000.

7. R. Touzi, A. Lopes, J. Bruniquel and P.W. Vachon, "Coherence Estimation for SAR Imagery," *IEEE Trans. GRS*, Vol. 37, No. 1, pp. 135-149, January 1999.

8. K.E. Mattar, A.L. Gray, D. Geudtner, and P.W. Vachon, "Interferometry for DEM and Terrain Displacement: Effects of Inhomogeneous Propagation," *Canadian Journal of Remote Sensing*, Vol. 25, No. 1, pp. 60-69, March 1999.

9. J.S. Lee, M.R. Grunes, G. de Grandi, "Polarimetric SAR Speckle Filtering and Its implication for Classification," *IEEE Transactions on Geoscience and Remote Sensing*, Vol. 37, No. 5, pp. 2363-2373, September 1999

10. J.S. Lee, K.P. Papathanassiou, T.L. Ainsworth, M.R. Grunes, A. Reigber, "A New Technique for Noise Filtering of SAR Interferometric Phase Images," *IEEE Transactions on Geoscience and Remote Sensing*, Vol. 26, No. 5, pp. 1456-1465, September 1998.

11. F.-H. Massmann, J. C. Neumayer, K. Raimondo, K. Enninghorst, and H. Li, "Quality of the D-PAF orbits before and after the inclusion of PRARE data," in *Proc. 3rd ERS Symp.: Space at the Service of our Environment*, Vol. 3, Florence, Italy, pp. 1655–1660, March 1997.

12. H. Rufenacht, R.J. Proulx, P.J. Cefola, "Improvement of RADARSAT Image localization," *The international symposium on Geomatics in the Era of RADARSAT (GER '97)*, Ottawa, Canada, May 25-30, 1997.

13. F. Gatelli, A. M. Guarnieri, F. Parizzi, P. Pasquali, C. Pratti and F. Rocca, "The Wavenumber Shift in SAR Interferometry," *IEEE Transactions on Geoscience and Remote Sensing,* Vol. 32, No. 4, pp. 855-865, July 1994.

14. J.M. Rignot and J.J. van Zyl, "Change detection techniques for ERS-1 SAR data," *IEEE Transactions on Geoscience and Remote Sensing*, Vol. 31, pp. 896-906, July 1993.

15. Environment Canada, "Ice Thickness Monthly Reports: Alert, NU," Metrological Services of Canada.

16. Hirose, T., Vachon, P.W., "Demonstration of ERS Tandem Mission SAR Interferometry for Mapping Land Fast Ice Evolution," *Canadian Journal of Remote Sensing*, Vol. 24, No 1. pp. 89-92, 1998.

Annexe A: List of ground truthing equipment and procedures

The GPS measurements were acquired using Garmin GPS-12 and/or Map-76 hand-held GPS receivers. For static positions (waypoints), the built-in average and estimated position error (EPE) were noted. For track measurements, the built-in track mode with (usually) a measurement every 2 seconds was used. In both cases, a Garmin commercial software product, Map Source with Canada Metro Guide maps, was used to download the logged data.

The corners used were constructed of 1/2" plywood with an aluminium skin (0.010 inches) bonded to the inside surfaces of the corner reflectors. The reflectors measured 1 m on a side with a hypotenuse of $\sqrt{2}$. A Sperry AngleStar digital protractor was used to set the corner's required inclination. The corner's azimuth was determined using one of the GPS receivers noted above.

Janice took most of the photographs with a Nikon D1 using a variety of different lenses, from 14 mm to 300 mm with extenders.

Annexe B: List of software

SAR and interferometric processing

MDA's "PGS" software was used to focus the raw RADARSAT-1 data and process the interferometric pair to a common Doppler centroid (thereby optimizing the coherence of the pair). In house software was used for most of the subsequent processing steps. "pgs_genhdr.c" generated the header information for the PGS output data file. "2pi_setup3.c" generated an ASCII parameter file containing the pertinent parameters. "estimate_coaresereg_rdsat.c" estimated the azimuth and range offset between the designated master and slave. This was verified using the display routine "img.c". After noting the azimuth and range offset in the parameter file, "coarsereg.c" generated complex master and slave image files registered to within a couple of pixels. "finereg_sm_rdsat.c" implemented sub-pixel registration of the slave to the master to within $1/8^{th}$ of a pixel. "fec_slave_radarsat.c" removed the flat-earth phase from the slave image. Finally "genint.c" generated the amplitudes, phase, and (boxcar filtered) coherence images and downsampled the data.

Coherence filtering

"cohmask_2l_19s.c" was used for coherence filtering for both the full resolution boxcar filtering and the 1x19 layer filter. "cohmask_2l_9s.c" was used for coherence filtering with the 1x9 layer filter.

Feature and trail mapping and evaluation

Given the satellite orbit data, "revamp_single.c" will map a single surveyed point (or series of points making up a track) from latitude, longitude, and height into the radar's range pixel and azimuth line perspective. This program also has utilities for geometric calibration of the radar scene. We then use an enhanced version of Atlantis Scientific's free imaging program, OpenEV (http://openev.sourceforge.net/), to display the surveyed points (or track) onto the scene magnitude, phase, or coherence image for evaluation. The statistics of the offset between the surveyed track and the imaged shoreline are generated using a series of Matlab utilities including "im2bw", "bwselect", "medfilt2", "contour".

Note: A large portion of this processing chain could be automated and streamlined, given sufficient interest.

DOCUMENT CONTROL DATA

(Security classification of title, body of abstract and indexing annotation must be entered when the overall document is classified)

1. ORIGINATOR (the name and address of the organization preparing the document. Organizations for whom the document was prepared, e.g. Establishment sponsoring a contractor's report, or tasking agency, are entered in section 8.)

Defence R&D Canada – Ottawa
Department of National Defence
Ottawa, Ontario, Canada K1A 0K2

2. SECURITY CLASSIFICATION (overall security classification of the document, including special warning terms if applicable)

UNCLASSIFIED

3. TITLE (the complete document title as indicated on the title page. Its classification should be indicated by the appropriate abbreviation (S,C or U) in parentheses after the title.)

Arctic shoreline delineation & feature detection using RADARSAT-1 interferometry: case study over Alert (U).

4. AUTHORS (Last name, first name, middle initial)

Mattar, Karim E., Gallop, Lloyd.

5. DATE OF PUBLICATION (month and year of publication of document)	6a. NO. OF PAGES (total containing information. Include Annexes, Appendices, etc.)	6b. NO. OF REFS (total cited in document)
December 2003	45	16

7. DESCRIPTIVE NOTES (the category of the document, e.g. technical report, technical note or memorandum. If appropriate, enter the type of report, e.g. interim, progress, summary, annual or final. Give the inclusive dates when a specific reporting period is covered.)

Technical Report

8. SPONSORING ACTIVITY (the name of the department project office or laboratory sponsoring the research and development. Include the address.)

Defence R&D Canada – Ottawa

9a. PROJECT OR GRANT NO. (if appropriate, the applicable research and development project or grant number under which the document was written. Please specify whether project or grant)	9b. CONTRACT NO. (if appropriate, the applicable number under which the document was written)
15eu17	

10a. ORIGINATOR'S DOCUMENT NUMBER (the official document number by which the document is identified by the originating activity. This number must be unique to this document.)	10b. OTHER DOCUMENT NOS. (Any other numbers which may be assigned this document either by the originator or by the sponsor)
DRDC Ottawa TR 2003-225	

11. DOCUMENT AVAILABILITY (any limitations on further dissemination of the document, other than those imposed by security classification)

(x) Unlimited distribution
( ) Distribution limited to defence departments and defence contractors; further distribution only as approved
( ) Distribution limited to defence departments and Canadian defence contractors; further distribution only as approved
( ) Distribution limited to government departments and agencies; further distribution only as approved
( ) Distribution limited to defence departments; further distribution only as approved
( ) Other (please specify):

12. DOCUMENT ANNOUNCEMENT (any limitation to the bibliographic announcement of this document. This will normally correspond to the Document Availability (11). However, where further distribution (beyond the audience specified in 11) is possible, a wider announcement audience may be selected.)

13. ABSTRACT (a brief and factual summary of the document. It may also appear elsewhere in the body of the document itself. It is highly desirable that the abstract of classified documents be unclassified. Each paragraph of the abstract shall begin with an indication of the security classification of the information in the paragraph (unless the document itself is unclassified) represented as (S), (C), or (U). It is not necessary to include here abstracts in both official languages unless the text is bilingual).

(U) We took advantage of the extensive ground truth carried out in and around Alert in 2002 to test the geometric calibration of RADARSAT-1, optimize the capability of RADARSAT-1 interferometry to delineate coastlines and riverbeds in an Arctic environment, and investigate the detection of various targets and feature of potential interest. Surveyed corner reflectors helped demonstrate that a ground reference point greatly improves the geometric calibration of RADARSAT-1 images. A new coherence filter was developed specifically optimized for coastline and riverbed delineation. GPS surveyed coastlines, mapped into radar perspective and calibrated using the surveyed corner reflectors, deviated from the coastline delineated using the coherence filter by less than 8 meters on average. Furthermore, assuming low decorrelation effects, coastlines and riverbeds are often clearly visible in the coherence image, potentially lending the delineation process much more readily to automation. However, RADARSAT-1's fine resolution mode proved too coarse to reliably detect trails, three crashed airplanes and various monuments in the area.

14. KEYWORDS, DESCRIPTORS or IDENTIFIERS (technically meaningful terms or short phrases that characterize a document and could be helpful in cataloguing the document. They should be selected so that no security classification is required. Identifiers such as equipment model designation, trade name, military project code name, geographic location may also be included. If possible keywords should be selected from a published thesaurus. e.g. Thesaurus of Engineering and Scientific Terms (TEST) and that thesaurus-identified. If it is not possible to select indexing terms which are Unclassified, the classification of each should be indicated as with the title.)

Interferometric SAR
Coastline delineation
Riverbed delineation
Coherence filter

Defence R&D Canada

Canada's leader in defence
and national security R&D

R & D pour la défense Canada

Chef de file au Canada en R & D
pour la défense et la sécurité nationale

DEFENCE DÉFENSE

www.drdc-rddc.gc.ca